# AN ABSTRACT OF THE THESIS OF

Jacqueline Wells for the degree of Master of Science in Environmental Engineering presented on June 7, 2021.

Title: Sediment Deposition Characteristics in Shallow Saturation Excess Overland Flow with Application to Bioswales and Construction of a Novel Bioswale Design for Improved Contaminant Removal from Stormwater

Abstract approved: _____

Tyler Radniecki

Over the last two decades, urban stormwater management has grown to include green infrastructure, such as bioswales. These systems were primarily designed to mitigate hydraulic peaking during rainstorms but were also found to remove particulate and dissolved contaminants. However, little is known about the fate of these particulate contaminants after depositing in bioswales. To better understand how the bed slope angle affects the deposition characteristics at a field scale, a two-foot-long flume was filled with soil from the OSU-Benton County Green Stormwater Infrastructure Research (OGSIR) facility. A fluorescent, paramagnetic sediment tracer was used to mimic silt sized particles carried by stormwater flows. A custom photographic hood with a specialized lens was used to image the flume surface after subsequent pulses of tracer slurry. The resulting images were analyzed to calculate the sediment trapping efficiency using the mean fluorescence intensity as a proxy for tracer mass. The sediment trapping efficiency estimates the amount of tracer that will be captured on the soil surface, thus removing particulate contaminants from the water. Samples of the flume effluent were collected for total suspended solids analysis to provide an approximate mass balance of deposited tracer with each slurry pulse. The bed slopes angles investigated were two, three, and four degrees. The experimental sediment trapping efficiencies were found to decrease with increasing bed slope angle, which indicates soils at greater bed slopes will be less capable of retaining particulate-associated contaminants. These results were also compared with two mathematical models from the literature.

While previous studies have shown that bioswales are also able to remove dissolved contaminants, there is great interest in improving the removal efficiencies, especially for heavy metals. One approach is to add commercial sorbents, which can have higher trapping affinities for a variety of contaminants. To investigate the impact of adding sorbents, a new bioswale design was created to mimic a treatment train with a traditional bioswale followed by two sets of sorbents: biochar and RemBind®. This new design utilizes the pre-existing OGSIR infrastructure, and its performance will serve as a comparison to the other traditional bioswales at the facility. The design, construction, and future sampling efforts are discussed to showcase the potential treatment performance improvement using this new treatment train system.

# Sediment Deposition Characteristics in Shallow Saturation Excess Overland Flow with Application to Bioswales and Construction of a Novel Bioswale Design for Improved Contaminant Removal from Stormwater

by
Jacqueline Wells

A THESIS

submitted to

Oregon State University

in partial fulfillment of
the requirements for the
degree of

Master of Science

Presented June 7, 2021
Commencement June 2021

Master of Science thesis of Jacqueline Wells presented on June 7, 2021

APPROVED:

Major Professor, representing Environmental Engineering

Head of the School of Chemical, Biological, and Environmental Engineering

Dean of the Graduate School

I understand that my thesis will become part of the permanent collection of Oregon State University libraries. My signature below authorizes release of my thesis to any reader upon request.

Jacqueline Wells, Author

# ACKNOWLEDGEMENTS

I would like to thank my advisor, Dr. Tyler Radniecki, and committee members Dr. Greg Wilson, Dr. Meghna Babbar-Sebens, and Dr. Jeff Nason for their patience, guidance, and mentorship as I developed and honed my field work and laboratory knowledge. I always enjoy learning new skills and I'm very grateful for their encouragement of my curiosity. I would also like to thank Dr. Sammy Rivera and all the students who were involved with the OGSIR treatment train project: Alisha Saduova, Carly Thorkildson, Julian Peter, and Lynne Sabourin. Their immense contributions with constructing and operating the new treatment train at OGSIR are what made it so successful. I'd like to thank my lab group and cohort for all their support, humor, and friendship as we've traveled through the program together. Finally, I'd like to thank my family and friends for all their love, moral support, and for cheering me throughout my life. I could not have achieved this accomplishment without them.

# TABLE OF CONTENTS

TABLE OF CONTENTS (Continued)

Page

# LIST OF FIGURES

# LIST OF FIGURES (Continued)

# LIST OF TABLES

Table Page

# 1. Introduction

## 1.1 Stormwater Characteristics

### 1.1.1 Overview

As communities continue to expand, the subsequent urbanization of native landscapes has led to increasing concerns about stormwater management.[1–3] Transitioning pervious landscapes to impervious ones and removing native vegetation to support growing infrastructure causes the disruption of hydraulic processes and degrades urban water quality.[1,2,4,5] Common impervious surfaces include roads, parking lots, and rooftops which cause significant increases in observed peak flows of stormwater runoff.[1,6,7] These excess peak flows often overwhelm conventional infrastructure (i.e. gutters and pipes)[6] and wastewater treatment facilities[2,5,8] and can result in flooding.[6] To overcome this issue, many cities have installed combined sewer overflow (CSO) systems to discharge any excess untreated runoff into natural water bodies.[1,5,8] While CSOs address the hydraulic flooding, they often negatively impact the quality of the receiving water body, which may be the source of the community's drinking water.[8–10] This is unsettling because stormwater runoff carries a variety of contaminants that can cause damaging human or ecological health effects.[7,9,11]

### 1.1.2 Typical Contaminants

The type and extent of the contaminants depends on a wide range of factors including rainfall characteristics, geological terrain, and land use.[12,13] Types of land uses include agriculture, residential, commercial, industrial, and developing urban areas.[7,10] The most common stormwater contaminants associated with these land uses are total suspended solids (TSS), nutrients (organic nitrogen and phosphorous species), dissolved organic matter (DOM), and trace metals (e.g. copper, zinc, lead, nickel).[9,11,14] These contaminants are typically classified into two groups based on their presence in stormwater: particulates and dissolved species.[9,15,16]

Particulate contaminants are mainly reflected in TSS measurements, where particles from eroding soil, roadways, and atmospheric deposition are washed off impervious surfaces during rainstorms.[1,14,17] These particulates can also have contaminants, such as heavy metals, bound to

their surfaces, allowing the particulates to facilitate the transport of other contaminants.[16,17] A particle's affinity for binding contaminants is often related to its size.[16,17] For example, heavy metals are most likely to be affiliated with silt sized particles (< 63 µm).[17,18] Treatment of these particles and any associated contaminants are effectively achieved through physical processes like sedimentation or filtration.[1,9]

Dissolved contaminants encompass a variety of chemical species, such as nutrients, heavy metals, DOM, and pesticides.[9,19] These also include polycyclic aromatic hydrocarbons (PAHs) and polychlorinated biphenyls (PCBs), which are considered emerging contaminants and have spurred many studies evaluating their transport through the environment.[9,14,16,19] The sources of dissolved contaminants are as varied as the contaminants, which can include vehicle components, vegetation, pavement, industrial spills, and fertilizers.[1,9] Typically, dissolved contaminants are more bioavailable, which makes them more likely to be taken up by plants, animals, and humans.[9,20] The resulting toxicity from bioaccumulation has underscored the importance of studying and remediating dissolved stormwater contaminants.[9] These contaminants can typically be treated by physical-chemical processes like adsorption onto specialized resins or via microbial transformations.[1,9]

## 1.2 Urban Stormwater Management

### 1.2.1 Green Stormwater Infrastructure

To address the degradation of urban stormwater quality and increased hydrological peak events, the US Environmental Protection Agency (US EPA) developed a set of best management practices (BMPs) in the 1990's.[21] This led to the implementation of low impact development (LID) and green stormwater infrastructure (GSI).[21] The main objective for LID and GSI projects is to mimic the natural pre-development conditions of a localized site.[22] This can be accomplished in several ways: 1) reducing hydrological peak flows, 2) sustaining groundwater recharge, 3) treating surface and stormwater contaminants, and 4) protecting critical environmental features like wetlands and riparian buffers.[22,23] One of the most well studied types of GSI is bioretention.[23] A few common examples are rain gardens and bioswales.[22] Bioretention systems can be defined as "small areas which are excavated and backfilled with a

mixture of high-permeability soil and organic matter designed to maximize infiltration and vegetative growth and are covered with native terrestrial vegetation." [21] The use of diverse, native vegetation is important to ensure the plants will survive the typical seasonal climates and can provide a habitat for local wildlife.[21,22,24] Unlike conventional stormwater infrastructure, bioretention systems are dynamic systems that can grow and change over time due to the incorporation of plants and soil-associated fauna.[25] When a bioretention system is initially constructed, the permeability of the soil will decrease due to compaction and surface clogging by fine particles.[26] As the plants and fauna, such as earthworms, become more established, the permeability will increase with time due to the creation of macropores and preferential flow paths through the subsurface.[26] These dynamic changes make bioretention systems difficult to design with predictable treatment performances since the efficacy for contaminant removal will vary over the lifetime of the system.[22,25]

### 1.2.2 Design Parameters for Bioswales

Bioswale designs are often site-specific and driven by the hydrological profile and the contaminant treatment goals.[22,23,25] These characteristics determine the selection of design parameters such as soil media, vegetation, and inclusion of other infrastructure, like underdrains.[22,23] In turn, these design choices affect the types of treatment processes (e.g. retention, filtration, adsorption, biodegradation) that can be implemented.[23,26] Bioswales can be installed in a variety of locations like medians, cul-de-sacs, and along highways and are typically sized to accommodate the initial flush of a storm event.[22,24,26]

When evaluating a potential site for a bioswale, the geology and soil characteristics will determine if an infiltration-style bioswale would be appropriate.[23] Bioswales can also be designed to allow stormwater runoff to recharge into the subsurface or keep it entirely isolated from the groundwater.[23,24] To isolate the runoff, plastic liners are added as waterproof barriers[24] and underdrains are added to provide an outlet for the water after percolating through the soil media.[23] Regardless of the choice of outlet, the goal is to reduce the exit velocities of the water from the system to mitigate erosion and prevent downstream flooding.[22,24] The soil media is often an engineered mixture selected based on several considerations like infiltration rate, ability

to sustain vegetation, and removal capability for expected hydrologic and contaminant loads.[23] It is also important to recognize the cradle-to-grave costs associated with purchasing, maintaining, and eventually disposing of the soil mixture.[23] A few performance recommendations for the soil media are 1) a maximum clay content of 5% and 2) passing 5-10 inches of rain per hour[24] or allowing infiltration of ponded water within 24 hours.[23] The corresponding ponding depth should be calculated using the influent hydrograph (e.g. flow rate, duration, total volume) and the volume storage capacity of the bioswale[23] with a maximum suggested ponding depth of 6-12 inches.[24] A final design element is the bed slope of the bioswale. According to the National Association of City Transportation Officials, the ideal longitudinal bed slopes of bioswales should be less than 4:1 (or 14-degrees)[24] to allow for sediments and particulate-associated contaminants to settle out.[22,24]

## 1.3 Sediment Tracers

### 1.3.1 Background

Efforts to understand the movement and fate of sediment through natural and anthropogenic processes has produced a growing field of research that can address modern sediment management issues.[27,28] Examples of these issues include eutrophication of water bodies, siltation in harbors, and transport of contaminated sediments.[28] "Particle" or "sediment tracing" is a technique that can be used to evaluate the transport pathways of sediments ranging in size from silt particles up to cobbles.[18,28] The labels or "signatures" applied to the particles allow them to be identified and "traced" in time and space during the study.[27,28] The first uses of this technique go back to the 1950s, where particles were tagged with radioactive labels.[28] Due to growing concerns of the environmental impact of releasing radioactive tracers, this type of tracer fell out of popular use in the United States.[28] It was eventually replaced with particles coated with fluorescent paints or dyes, which are still widely used today.[18,28] Particle tracers in contemporary studies are classified into two groups based on the tracer's origin, either as natural or synthetic particles.[28] Generally, natural particles are more commonly used because it is relatively easy to certify that the tracer hydraulic properties match those of the natural sediment.[28] While tracers are typically only tagged with one signature, a new type of synthetic

tracers have been produced that utilize a "dual-signature." [18,28] One example is a particle with a paramagnetic core and coated with a fluorescent dye.[18,28] The fluorescent dye is used for *in situ* tracking of the particle while the paramagnetic properties allow for easy separation from native sediment samples with a permanent or electro-magnet.[18,27,28]

### 1.3.2 Experimental Principles

There are three underlying assumptions that must be satisfied for a successful tracer study: 1) the tracer must mimic the hydraulic behaviors of the sediment of interest so the transport phenomena to be accurately replicated, 2) the tracer properties will not change over time and the tracer signature can be monitored, and 3) the tracer will not interfere with the natural transportation pathway.[28] If these assumptions can be met with confidence, then a study can be designed and completed using five steps.[18] The first step is performing a background survey where the natural particle properties (e.g. size, density, settling velocity) are determined. The next step is designing the tracer to match the natural properties and adding the desired signature. The manufacturers will also conduct similarity testing to verify the physical and hydraulic properties mimic the behavior of the natural particles. The third step is determining a method for distributing the particle tracers into the study environment. This will be site and study-specific, but some examples include creating a point-source plume, depositing tracer on dry land, and continuous slurry injection. The fourth step is collecting samples of the tracer through space and time using a method appropriate for the tracer signature. The final step is analyzing the samples to determine the amount of tracer present on a dry mass basis. There are several options for quantifying the tracer mass, including spectrofluorometric analysis and digital imaging via the sedimentation of the particles. Note, while the tracer mass can be quantified, there will be some or even significant loss of the tracer once released into the environment because it is impossible to sample everywhere at every time.[27] Although this loss makes it difficult to conduct a complete a mass balance on the system, researchers can still gain valuable insight into the spatial and temporal behavior of the transport pathways.[27]

### 1.3.3 Field Applications

Particle tracer studies have been conducted at many different geographical scales from laboratory flumes to large catchments (> 100 hectares).[29] Two of the most common field applications for tracers are in 1) oceans and estuaries[18,30–37] and 2) rivers and streams.[38–45] There are many sediment-transport related questions that can be investigated using tracers including sediment deposition,[30–32,34,35,37,44,46] sediment resuspension,[30,31,33,43] sources of sediments,[34,35,39,47] and transport due to erosion.[39,45,48,49] Tracers can also be used to evaluate how temporal changes affect sediment pathways on a seasonal basis[32,33,38] or on an event basis.[29,32,39,40,43,49] Field studies are not limited to small grain particles;[18,30,31,33,38,39,45–47] some investigate the transport of sands,[34–36,50] gravels,[41] and cobbles.[40] One field application that is far less studied is the transport of sediments due to storm events. Some papers have looked at sediment erosion due to runoff in agricultural settings,[48,49] while others have examined sediment transport via traditional stormwater infrastructure.[46,47,50] Recently, there have been a few studies investigating the sediment transport in GSI systems, specifically grassed swales.[12,51–53]

## 1.4 Thematic Connection of Thesis Chapters

Effective stormwater management is crucial to maintaining the environmental and human health of our communities by protecting the quality of natural water sources. Therefore, it is important to continue expanding the knowledge of stormwater contaminant removal processes and innovating current bioswale designs to achieve greater treatment efficiencies. The two chapters included in this thesis will 1) provide results from a sediment tracer study evaluating the sediment transport in bioswales and 2) present a novel bioswale treatment train design incorporating sorbent amendment for improving contaminant removal at the OSU-Benton County Green Stormwater Infrastructure Research (OGSIR) facility. The OGSIR facility consists of three bioretention (bioswale) “cells” for testing different treatment technologies for a variety of stormwater contaminants.

The common thread between these two chapters are their direct applications to OGSIR. For the sediment tracer study, determining the sediment trapping efficiency of OGSIR soil for particles known to be associated with stormwater contaminants illuminates the processes by which these

particles can be removed in the bioretention systems at the site. If these particles are not initially trapped on the soil beds, then understanding the particles' transport through the bioswale can reveal where the particles do deposit, or if they are carried back out into the environment. The new treatment train design focuses on improving the removal of dissolved contaminants by incorporating commercial sorbents that have greater trapping affinities than the native soil. Adding a media with stronger or permanent binding capabilities reduces the risk of the contaminants leaching out of the system. Studying the removal processes for particulate and dissolved contaminants through the tracer experiments and the new treatment train design, provides a comprehensive evaluation of the fate and transport of these contaminants at the OGSIR field site.

## 1.5 Bibliography

(1) Barbosa, A. E.; Fernandes, J. N.; David, L. M. Key Issues for Sustainable Urban Stormwater Management. *Water Research* **2012**, *46* (20), 6787–6798. https://doi.org/10.1016/j.watres.2012.05.029.

(2) Fletcher, T. D.; Andrieu, H.; Hamel, P. Understanding, Management and Modelling of Urban Hydrology and Its Consequences for Receiving Waters: A State of the Art. *Advances in Water Resources* **2013**, *51*, 261–279. https://doi.org/10.1016/j.advwatres.2012.09.001.

(3) LeFevre, N.-J.; Watkins Jr., D. W.; Gierke, J. S.; Brophy-Price, J. Hydrologic Performance Monitoring of an Underdrained Low-Impact Development Storm-Water Management System. *Journal of Irrigation and Drainage Engineering* **2010**, *136* (5).

(4) Muerdter, C.; Wong, C. K.; LeFevre, G. H. Emerging Investigator Series: The Role of Vegetation in Bioretention for Stormwater Treatment in the Built Environment: Pollutant Removal, Hydrologic Function, and Ancillary Benefits; 2018. https://doi.org/10.1039/C7EW00511C.

(5) Chen, J.; Theller, L.; Gitau, M. W.; Engel, B. A.; Harbor, J. M. Urbanization Impacts on Surface Runoff of the Contiguous United States. *Journal of Environmental Management* **2017**, *187*, 470–481. https://doi.org/10.1016/j.jenvman.2016.11.017.

(6) Meierdiercks, K. L.; Smith, J. A.; Baeck, M. L.; Miller, A. J. Analyses of Urban Drainage Network Structure and Its Impact on Hydrologic Response1. *JAWRA Journal of the American Water Resources Association* **2010**, *46* (5), 932–943. https://doi.org/10.1111/j.1752-1688.2010.00465.x.

(7) Nayeb Yazdi, M.; Sample, D. J.; Scott, D.; Wang, X.; Ketabchy, M. The Effects of Land Use Characteristics on Urban Stormwater Quality and Watershed Pollutant Loads. *Science of The Total Environment* **2021**, *773*, 145358. https://doi.org/10.1016/j.scitotenv.2021.145358.

(8) Walsh, C. J.; Roy, A. H.; Feminella, J. W.; Cottingham, P. D.; Groffman, P. M.; Morgan, R. P. The Urban Stream Syndrome: Current Knowledge and the Search for a Cure. *Journal of the North American Benthological Society* **2005**, *24* (3), 706–723. https://doi.org/10.1899/04-028.1.

(9) LeFevre, G. H.; Paus, K. H.; Natarajan, P.; Gulliver, J. S.; Novak, P. J.; Hozalski, R. M. Review of Dissolved Pollutants in Urban Storm Water and Their Removal and Fate in Bioretention Cells. *J. Environ. Eng.* **2015**, *141* (1), 04014050. https://doi.org/10.1061/(ASCE)EE.1943-7870.0000876.

(10) Environmental Protection Agency (EPA). *Environmental Impacts of Stormwater Discharges*; EPA 841-R-92-001; US EPA: Washington DC, USA, 1992; p 45.

(11) Masoner, J. R.; Kolpin, D. W.; Cozzarelli, I. M.; Barber, L. B.; Burden, D. S.; Foreman, W. T.; Forshay, K. J.; Furlong, E. T.; Groves, J. F.; Hladik, M. L.; Hopton, M. E.; Jaeschke, J. B.; Keefe, S. H.; Krabbenhoft, D. P.; Lowrance, R.; Romanok, K. M.; Rus, D. L.; Selbig, W. R.; Williams, B. H.; Bradley, P. M. Urban Stormwater: An Overlooked Pathway of Extensive Mixed Contaminants to Surface and Groundwaters in the United States. *Environ. Sci. Technol.* **2019**, *53* (17), 10070–10081. https://doi.org/10.1021/acs.est.9b02867.

(12) Deletic, A. Modelling of Water and Sediment Transport over Grassed Areas. *Journal of Hydrology* **2001**, *248* (1), 168–182. https://doi.org/10.1016/S0022-1694(01)00403-6.

(13) Li, J.; Jiang, C.; Lei, T.; Li, Y. Experimental Study and Simulation of Water Quality Purification of Urban Surface Runoff Using Non-Vegetated Bioswales. *Ecological Engineering* **2016**, *95*, 706–713. https://doi.org/10.1016/j.ecoleng.2016.06.060.

(14) Müller, A.; Österlund, H.; Marsalek, J.; Viklander, M. The Pollution Conveyed by Urban Runoff: A Review of Sources. *Science of The Total Environment* **2020**, *709*, 136125. https://doi.org/10.1016/j.scitotenv.2019.136125.

(15) Zgheib, S.; Moilleron, R.; Saad, M.; Chebbo, G. Partition of Pollution between Dissolved and Particulate Phases: What about Emerging Substances in Urban Stormwater Catchments? *Water Research* **2011**, *45* (2), 913–925. https://doi.org/10.1016/j.watres.2010.09.032.

(16) Grant, S. B.; Rekhi, N. V.; Pise, N. R.; Reeves, R. L.; V, F. *A REVIEW OF THE CONTAMINANTS AND TOXICITY ASSOCIATED WITH PARTICLES IN STORMWATER RUNOFF*; California Department of Transportation, 2003.

(17) Baum, P.; Kuch, B.; Dittmer, U. Adsorption of Metals to Particles in Urban Stormwater Runoff—Does Size Really Matter? *Water* **2021**, *13* (3), 309. https://doi.org/10.3390/w13030309.

(18) Black, K.; Sloan, J.; Gries, T. Everything Goes Somewhere; Tracking the Movement of Contaminated Sediments in an Industrialised Estuary Using Dual Signature Sediment Tracers. *EPJ Web of Conferences* **2013**, *50*, 04001. https://doi.org/10.1051/epjconf/20135004001.

(19) Pitt, R.; Field, R.; Lalor, M.; Brown, M. Urban Stormwater Toxic Pollutants: Assessment, Sources, and Treatability. *Water Environment Research* **1995**, *67* (3), 260–275.

(20) Kayhanian, M.; Fruchtman, B. D.; Gulliver, J. S.; Montanaro, C.; Ranieri, E.; Wuertz, S. Review of Highway Runoff Characteristics: Comparative Analysis and Universal Implications. *Water Res* **2012**, *46* (20), 6609–6624. https://doi.org/10.1016/j.watres.2012.07.026.

(21) Roy-Poirier, A.; Champagne, P.; Filion, Y. Review of Bioretention System Research and Design: Past, Present, and Future. *Journal of Environmental Engineering* **2010**, *136* (9), 878–889. https://doi.org/10.1061/(ASCE)EE.1943-7870.0000227.

(22) Environmental Protection Agency (EPA). *Low Impact Development (LID) A Literature Review*; EPA-841-B-00-005; US EPA: Washington DC, USA, 2000; p 41.

(23) Davis, A. P.; Hunt, W. F.; Traver, R. G.; Clar, M. Bioretention Technology: Overview of Current Practice and Future Needs. *Journal of Environmental Engineering* **2009**, *135* (3), 109–117. https://doi.org/10.1061/(ASCE)0733-9372(2009)135:3(109).

(24) National Association of City Transportation Officials. Bioswales https://nacto.org/publication/urban-street-design-guide/street-design-elements/stormwater-management/bioswales/.

(25) Greene, A. M.; Hutchinson, S. L.; Christianson, R.; Moore, T. L. Impacts of Biota on Bioretention Cell Performance during Establishment in the Midwest. In *World Environmental and Water Resources Congress 2009*; American Society of Civil Engineers: Kansas City, Missouri, United States, 2009; pp 1–13. https://doi.org/10.1061/41036(342)448.

(26) Hatt, B. E.; Fletcher, T. D.; Deletic, A. Hydrologic and Pollutant Removal Performance of Stormwater Biofiltration Systems at the Field Scale. *Journal of Hydrology* **2009**, *365* (3–4), 310–321. https://doi.org/10.1016/j.jhydrol.2008.12.001.

(27) Black, K. S. Using Sediment Tracers to Map Sediment Transport Pathways: A Primer. Partrac, Ltd 2013.

(28) Black, K. S.; Athey, S.; Wilson, P.; Evans, D. The Use of Particle Tracking in Sediment Transport Studies: A Review. *Geological Society, London, Special Publications* **2007**, *274* (1), 73–91. https://doi.org/10.1144/GSL.SP.2007.274.01.09.

(29) Guzmán, G.; Quinton, J. N.; Nearing, M. A.; Mabit, L.; Gómez, J. A. Sediment Tracers in Water Erosion Studies: Current Approaches and Challenges. *J Soils Sediments* **2013**, *13* (4), 816–833. https://doi.org/10.1007/s11368-013-0659-5.

(30) Giffin, D.; Corbett, D. R. Evaluation of Sediment Dynamics in Coastal Systems via Short-Lived Radioisotopes. *Journal of Marine Systems* **2003**, *42* (3), 83–96. https://doi.org/10.1016/S0924-7963(03)00068-X.

(31) Feng, H.; Cochran, J. K.; Hirschberg, D. J. 234Th and 7Be as Tracers for the Transport and Dynamics of Suspended Particles in a Partially Mixed Estuary. *Geochimica et Cosmochimica Acta* **1999**, *63* (17), 2487–2505. https://doi.org/10.1016/S0016-7037(99)00060-5.

(32) Palinkas, C. M.; Nittrouer, C. A.; Wheatcroft, R. A.; Langone, L. The Use of 7Be to Identify Event and Seasonal Sedimentation near the Po River Delta, Adriatic Sea. *Marine Geology* **2005**, *222–223*, 95–112. https://doi.org/10.1016/j.margeo.2005.06.011.

(33) Roos, P.; Valeur, J. R. A Sediment Trap and Radioisotope Study to Determine Resuspension of Particle Reactive Substances in the Sound between Sweden and Denmark. *Continental Shelf Research* **2006**, *26* (4), 474–487. https://doi.org/10.1016/j.csr.2006.01.001.

(34) Su, C.-C.; Huh, C.-A. 210Pb, 137Cs and 239,240Pu in East China Sea Sediments: Sources, Pathways and Budgets of Sediments and Radionuclides. *Marine Geology* **2002**, *183* (1), 163–178. https://doi.org/10.1016/S0025-3227(02)00165-2.

(35) Du, J.; Wu, Y.; Huang, D.; Zhang, J. Use of 7Be, 210Pb and 137Cs Tracers to the Transport of Surface Sediments of the Changjiang Estuary, China. *Journal of Marine Systems* **2010**, *82* (4), 286–294. https://doi.org/10.1016/j.jmarsys.2010.06.003.

(36) Miller, I. M.; Warrick, J. A.; Morgan, C. Observations of Coarse Sediment Movements on the Mixed Beach of the Elwha Delta, Washington. *Marine Geology* **2011**, *282* (3), 201–214. https://doi.org/10.1016/j.margeo.2011.02.012.

(37) Moritz, H.; Puckette, T.; Marsh, J.; Boudreau, R.; Siipola, M.; Ott, M. *Utilizing Sediment Tracer Studies to Evaluate Transport Pathways at the Mouth of the Columbia River, USA*; ARMY ENGINEER DISTRICT PORTLAND OR, 2011.

(38) Koch, G. R.; Hagerthey, S.; Childers, D. L.; Gaiser, E. Examining Seasonally Pulsed Detrital Transport in the Coastal Everglades Using a Sediment Tracing Technique. *Wetlands* **2014**, *34* (1), 123–133. https://doi.org/10.1007/s13157-013-0388-y.

(39) Wilkinson, S. N.; Wallbrink, P. J.; Hancock, G. J.; Blake, W. H.; Shakesby, R. A.; Doerr, S. H. Fallout Radionuclide Tracers Identify a Switch in Sediment Sources and Transport-Limited

Sediment Yield Following Wildfire in a Eucalypt Forest. *Geomorphology* **2009**, *110* (3), 140–151. https://doi.org/10.1016/j.geomorph.2009.04.001.

(40) Phillips, C. B.; Jerolmack, D. J. Dynamics and Mechanics of Bed-Load Tracer Particles. *Earth Surface Dynamics* **2014**, *2* (2), 513–530. http://dx.doi.org.ezproxy.proxy.library.oregonstate.edu/10.5194/esurf-2-513-2014.

(41) Vázquez-Tarrío, D.; Recking, A.; Liébault, F.; Tal, M.; Menéndez-Duarte, R. Particle Transport in Gravel-Bed Rivers: Revisiting Passive Tracer Data. *Earth Surface Processes and Landforms* **2019**, *44* (1), 112–128. https://doi.org/10.1002/esp.4484.

(42) Brambilla, D.; Papini, M.; Longoni, L. Temporal and Spatial Variability of Sediment Transport in a Mountain River: A Preliminary Investigation of the Caldone River, Italy. *Geosciences* **2018**, *8* (5), 163. http://dx.doi.org.ezproxy.proxy.library.oregonstate.edu/10.3390/geosciences8050163.

(43) Rowntree, K. M.; van der Waal, B. W.; Pulley, S. Magnetic Susceptibility as a Simple Tracer for Fluvial Sediment Source Ascription during Storm Events. *Journal of Environmental Management* **2017**, *194*, 54–62. https://doi.org/10.1016/j.jenvman.2016.11.022.

(44) Cain, A.; MacVicar, B. Field Tests of an Improved Sediment Tracer Including Non-Intrusive Measurement of Burial Depth. *Earth Surface Processes and Landforms* **2020**, *45* (14), 3488–3495. https://doi.org/10.1002/esp.4980.

(45) Riedel, M. S. Quantifying Trail Erosion and Stream Sedimentation with Sediment Tracers. *Second Interagency Conference on Research in the Watersheds, May 16-18, 2006. 9 p.* **2006**.

(46) Spencer, K. L.; Droppo, I. G.; He, C.; Grapentine, L.; Exall, K. A Novel Tracer Technique for the Assessment of Fine Sediment Dynamics in Urban Water Management Systems. *Water Research* **2011**, *45* (8), 2595–2606. https://doi.org/10.1016/j.watres.2011.02.012.

(47) Yin, C.; Li, L. An Investigation on Suspended Solids Sources in Urban Stormwater Runoff Using 7Be and 210 Pb as Tracers. *Water Science and Technology* **2008**, *57* (12), 1945–1950. http://dx.doi.org.ezproxy.proxy.library.oregonstate.edu/10.2166/wst.2008.274.

(48) Guzmán, G.; Laguna, A.; Cañasveras, J. C.; Boulal, H.; Barrón, V.; Gómez-Macpherson, H.; Giráldez, J. V.; Gómez, J. A. Study of Sediment Movement in an Irrigated Maize–Cotton System Combining Rainfall Simulations, Sediment Tracers and Soil Erosion Models. *Journal of Hydrology* **2015**, *524*, 227–242. https://doi.org/10.1016/j.jhydrol.2015.02.033.

(49) Guzmán, G.; Barrón, V.; Gómez, J. A. Evaluation of Magnetic Iron Oxides as Sediment Tracers in Water Erosion Experiments. *CATENA* **2010**, *82* (2), 126–133. https://doi.org/10.1016/j.catena.2010.05.011.

(50) Boving, T.; Lewis, T.; Siswoyo, E. An Innovative Approach to Tracking Sediment Transport along Roads. *MATEC Web Conf.* **2019**, *280*, 04001. https://doi.org/10.1051/matecconf/201928004001.

(51) Pearce, R. A.; Trlica, M. J.; Leininger, W. C.; Smith, J. L.; Frasier, G. W. Efficiency of Grass Buffer Strips and Vegetation Height on Sediment Filtration in Laboratory Rainfall Simulations. *Journal of Environmental Quality* **1997**, *26* (1), 139.

(52) Robinson, C. A.; Ghaffarzadeh, M.; Cruse, R. M. Vegetative Filter Strip Effects on Sediment Concentration in Cropland Runoff. *Journal of Soil and Water Conservation* **1996**, *51* (3), 227–231.

(53) Ligdi, E.; Morgan, R. Contour Grass Strips: A Laboratory Simulation of Their Role in Soil Erosion Control. *Soil Technology* **1995**, *8* (2), 109–117. https://doi.org/10.1016/0933-3630(95)00011-0.

# 2. Sediment Deposition Characteristics in Shallow Saturation Excess Overland Flow with Application to Bioswales

## 2.1 Introduction

Over the last several decades there has been a growing body of research for understanding the principles of contaminant transport and to create models for predicting their fate in the environment. Contaminants from non-point sources, like runoff from agricultural and urbanized areas, have become major contributors to the pollution found in surface water and groundwater.[1,2] These contaminants can be present as dissolved constituents or affiliated with naturally occurring particles like clay or silt.[1,3] To mitigate the hydraulic and pollution concerns associated with stormwater runoff, urban areas have implemented green infrastructure, such as bioswales, as a best management practice (BMP) for stormwater.[4] While there has been research on the sediment transport in a variety of urban stormwater infrastructure, like retention ponds[2,5,6] and grassed areas,[1,7,8] there is a lack of studies related to field-scale bioswales.

To address this knowledge gap, this study utilized sediment tracers to track sediment transport and deposition in a field-scale flume to mimic the soil bank of a bioswale. Sediment tracers are typically created by adding a "signature" to natural or artificial particles in order to track them in time and space.[9] For this study, we relied on dual-signature (fluorescent and paramagnetic) silt sized tracers.[10] Tracers have been applied to many field environments, most often in oceans, estuaries, rivers, and streams.[9–11] However, use of these tracers in extremely shallow aquatic environments, like stormwater runoff, is far less common. Stormwater runoff is best described as shallow "saturation excess overland flow" (SEOF).[12] This process occurs when soils are completely saturated and any additional rainfall will result in overland flow.[12,13]

There are many factors that will influence the sediment deposition within stormwater runoff. These include soil properties (infiltration, roughness), geological terrain (bed length and slope), type and extent of vegetation, sediment particle characteristics (size and density), and rainfall (intensity, duration, sediment inflow rate).[1] While the effects of bed slope have been studied in grassy areas,[14,15] there are only a few articles that evaluate slope effects for bare soil.[16] A key parameter used to describe the level of sediment deposition into the bed is the trapping efficiency ($\lambda$) [1/m].[1,17,18] The trapping efficiency is defined as the ratio of measured sediment deposition

to the amount of sediment that is capable of deposition per unit length.[17] Models utilizing λ have been used for studies of fine sediment deposition by infiltration into coarse sand-gravel beds,[1,19–23] effectively treating the bed as a filtering medium. In these models, cumulative surface deposition will decrease exponentially with distance, such that fitting an exponential curve to a plot of sediment concentration vs length will yield an e-folding length scale of $L_x=1/\lambda$. However, since the physical aspects of sediment deposition are wrapped into the λ parameter, it's been difficult for researchers to create a universal theory for this phenomenon. The lack of a universal theory is also due to the wide range of depositional processes (like deposition via particle settling, cohesive processes, or straining) that may have different levels of importance for a given setting.[24] In the case of silt sized particle deposition (which will be examined in this study), we hypothesize that particle trapping will be mostly due to straining rather than a filter cake or via physio-chemical mechanisms.[24] To our knowledge, trapping rate parameters have not been extensively studied for the unique hydraulic conditions associated with SEOF. A notable exception is a study by Deletic (2001), who found that a trapping-rate-based model could provide a reasonable fit to experimental data of sediment trapping on impermeable grass strips.[1] Extension of these results to permeable-bed SEOF flow is a key contribution of the present work.

The goals of this study are 1) determine the sediment trapping efficiency, λ, under shallow SEOF that mimics conditions at a local bioswale field site, and 2) evaluate the fit of experimental trapping efficiencies with consideration of potential hydraulic and sediment conditions that could affect sediment deposition.

## 2.2 Methods and Materials

### 2.2.1 Particle Deposition Theory

For the purposes of this paper, we will focus on two models: one introduced by Deletic[1] for flow over impermeable grass filter strips, and the second based on deposition probability, a commonly used concept originally due to Einstein & Krone (1962),[25] which will be referred to here as the Einstein-Krone model.

The Deletic model[1] begins with Equation 2.1, which describes a mass balance of suspended sediment,

$$\frac{\partial\left(\frac{hq_{s,s}}{q}\right)}{\partial t} + \frac{\partial q_{s,s}}{\partial x} = Dis\frac{\partial^2\left(\frac{hq_{s,s}}{q}\right)}{\partial x^2} - \lambda_s q_{s,s} \quad (2.1)$$

Here, h is the depth of flow [m], $q_{s,s}$ is the sediment loading rate of fraction s per unit width [g $s^{-1}$ $m^{-1}$], q is overland flow rate per unit width [$m^2$ $s^{-1}$], Dis is the dispersion coefficient [$m^2$ s], and $\lambda_s$ is the trapping efficiency for fraction s per unit length [$m^{-1}$]. For the present experiments, we will neglect dispersion and assume h/q is a constant since there will be a constant flow rate and flow depth. Thus, equation (2.1) can be simplified to:

$$\frac{\partial q_{s,s}}{\partial x} = -\lambda_s q_{s,s} \quad (2.2)$$

Deletic proposes a series of equations leading to a model for $\lambda_s$:

$$\text{Manning's Equation: } q = \frac{\sqrt{S}}{n}h^{5/3} \quad (2.3)$$

Here, S is the bed slope gradient [-] and n is the Manning's coefficient [s $m^{-1/3}$]. The Manning's coefficient for firm soil is 0.02.[26] This is used to calculate the flow depth from the known q. Next, the particle fall number ($N_{f,s}$) is calculated:

$$N_{f,s} = \frac{lV_s}{hV} \quad (2.4)$$

where l is the length of the grass strip [m], $V_s$ is the Stokes' settling velocity of the particles with diameter $d_s$ [m $s^{-1}$], and V is the average mean flow velocity. To calculate $V_S$ and V:

$$V_s = \frac{g}{18\mu}(\rho_s - \rho){d_s}^2 \quad (2.5)$$

$$V = \frac{q}{B_o h} \quad (2.6)$$

Here, g is gravitational acceleration 9.81 [m $s^2$], μ is the dynamic viscosity of water [kg $s^{-1}$ $m^{-1}$], $\rho_s$ is the particle density [kg $m^{-3}$], ρ is the density of water [kg $m^{-3}$], $d_s$ is the particle diameter [m], and $B_o$ is the open flow width per unit width [-]. The trapping efficiency for the sediment fraction s ($T_{r,s}$) [-] is related to $N_{f,s}$ using a semi-empirical equation determined by Deletic:

$$T_{r,s} = \frac{{N_{f,s}}^{0.69}}{{N_{f,s}}^{0.69}+4.95} \quad (2.7)$$

Finally, the $\lambda_s$ is found by:

$$\lambda_s = \frac{T_{r,s}\left(\frac{lV_s}{Vh}\right)}{l} \tag{2.8}$$

where $T_{r,s}$ is a function of ($lV_s/Vh$).

In summary, the Deletic model uses dimensional considerations to define the parameter $N_{f,s}$, which was fitted to experimental data to obtain equation (2.7). Other models attempt to predict $\lambda_s$ from physical principles. A common assumption is that suspended particles reach the bed at a rate according to their settling velocity, with a fixed fraction of those particles becoming deposited. Unlike the Deletic model, the Einstein-Krone model[20] does consider the resuspension of deposited particles. The equation for accounting for this process in terms of suspended particle concentration is:

$$\frac{dc}{dt} = \frac{-m_0 v_0 v_s p}{y} \tag{2.9}$$

Here, c is suspended sediment concentration [kg $L^{-1}$], t is elapsed time [s], $m_0$ is the individual particle mass, $v_0$ is the number of primary particles per volume [$m^{-3}$], $v_s$ is the settling velocity [m $s^{-1}$], y is water depth, and p is the overall probability of a particle sticking to the soil bed. In this case, p does not differentiate between particles that don't deposit and those that are resuspended after depositing. In the Einstein-Krone model, the physical property of p stems from the bed and critical shear forces acting on the soil bed as particles suspended in the water flow over it. Given that $m_0 v_0$=c and if $v_s$ is independent of c and t, Equation 2.9 can be solved:

$$\frac{c}{c_0} = e^{\left(\frac{-ptv_s}{y}\right)} \tag{2.10}$$

Aspects of these two models were incorporated into a new, simplistic model that accounts for the Vs, V, and h from the Deletic model and the concentration and probability parameters from Einstein-Krone. Since the rate of deposition (D) [# particles settling/second] is equal to the suspended sediment concentration times the settling velocity, we can also include the probability of a particle depositing on the soil surface. Given that the concentration is equal to the flux of the particles divided by the flow velocity and depth of flow, we can get the following equations:

$$D = cV_s p = q\left(\frac{V_s p}{Vh}\right) \tag{2.11}$$

$$D = \frac{dq_s}{dx} = -\lambda q \tag{2.12}$$

$$\frac{dq}{dx} = -\left(\frac{V_s P}{Vh}\right) q \tag{2.13}$$

where $q_s$ is the sediment transport rate [kg $m^{-1}$ $s^{-1}$]. Equation 2.13 provides a physical basis for the trapping efficiency. Solving Equation 2.12 yields:

$$q_s(x) = q_{s,0} e^{-\lambda x} \tag{2.14}$$

where $q_0$ is the sediment transport rate at the flume inlet at x = 0. $q_0$ is calculated by:

$$q_{s,0} = \frac{Mq}{W} \tag{2.15}$$

where M is the sediment load at the inlet [kg $m^{-3}$] and W is the flume width [m].

The deposition of sediment vs. downstream distance (d(x)) can in turn be derived as:

$$d(x) = \frac{\partial q_s}{\partial x} = -\lambda q_{s,0} e^{-\lambda x} \tag{2.16}$$

To determine the total deposition ($D_{tot}$) along a given length (L) [m], Equation 2.16 can be integrated:

$$D_{tot} = W \int_0^L \frac{\partial q_s}{\partial x} dx = W q_0 \left(1 - e^{-\lambda L}\right) \tag{2.17}$$

This yields the amount of sediment removed from the flow per unit time [kg $s^{-1}$] and will be used to determine a mass balance for the sediment deposition process in the flume experiments.

### 2.2.2 Materials Specifications

The experiments utilized a single-lane flume constructed from 3/8" thick PVC plastic. The bottom of the flume utilized this same material, so it was impermeable to water. The flume dimensions were 48" long, 12" wide, and 12" tall with 6" walls on the ends of the flume. Slats were added to the bottom of the flume to provide extra friction for the soil when the flume was inclined. A clear tray with four injection nozzles was attached at the head of the flume. This was connected via 3/8" plastic tubing to a diaphragm slurry pump. This pump delivered a prepared tracer slurry from a 5-gallon bucket to the tray, which then overflowed into the flume to create an inlet stream of tracer-laden water while creating minimal disturbance to the flume surface sediment. Due to the rapid settling of the tracer particles, an electric paint mixer was

installed to continually suspend the slurry in the 5-gallon bucket. A small container was placed under the end of the flume to capture the effluent run-off for total suspended solids analysis. See Figure 2.1 for a photo of the experimental set-up.

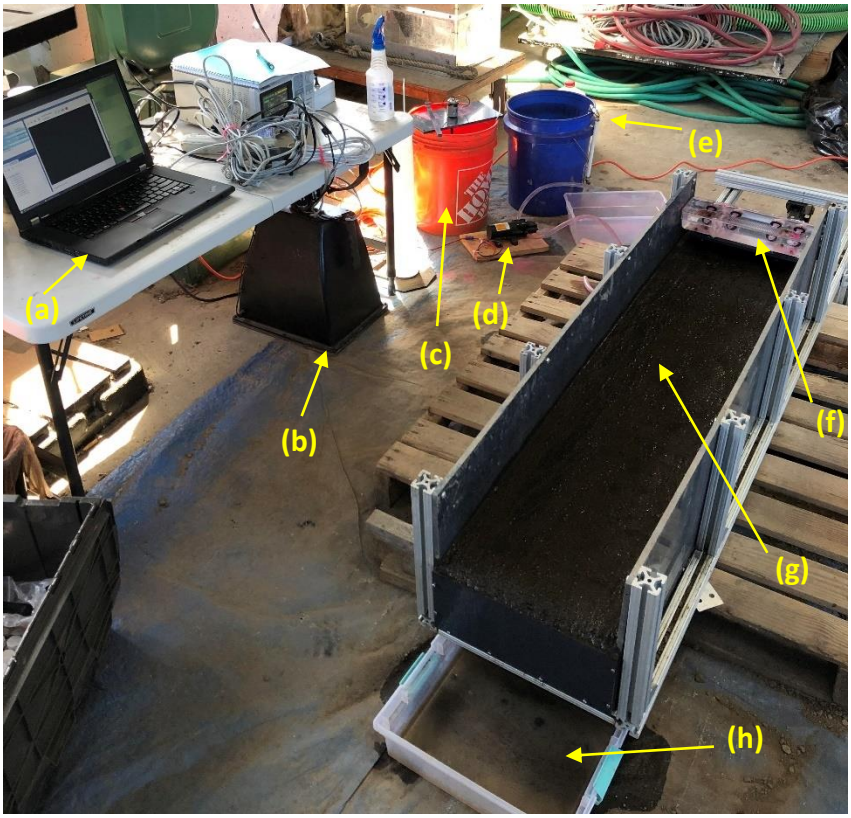


**Figure 2.1.** Photo of the experimental set-up. (**a**) Laptop for capturing images from photographic hood. (**b**) Photographic hood. (**c**) 5-gallon bucket with tracer slurry and electric paint mixer. (**d**) Diaphragm slurry pump. (**e**) 5-gallon bucket with tap water. (**f**) Tracer tray with four nozzles. (**g**) Flume with compacted soil. (**h**) container for capturing effluent run-off.

The tracers used for these experiments were paramagnetic, fluorescent, silt sized particles with $d_{50}$ of 40 µm that had an excitation band of 250-550 nm and a peak fluorescence emission frequency of 610 nm.[27] Figure 2.2 shows the particle size distribution of the tracer. A photographic hood was developed to illuminate the fluorescent particles on the surface of the flume, using their intensity as a proxy for their surficial concentration. This consisted of a black hard-shelled dome with a mounted Point Gray BlackFlyS camera (2448 by 2048 pixels, 8 mm focal length), pointing directly down onto the sediment bed from a height of 12.2". The photo

sample area was 10.2” long and 7.5” wide. The camera was fitted with a bandpass filter of center wavelength 610 nm and bandwidth of 10 nm. A black light ring was used to illuminate the bed surface with a nominal wavelength of 365 nm. See Figure 2.3 for images of the photographic hood set-up.

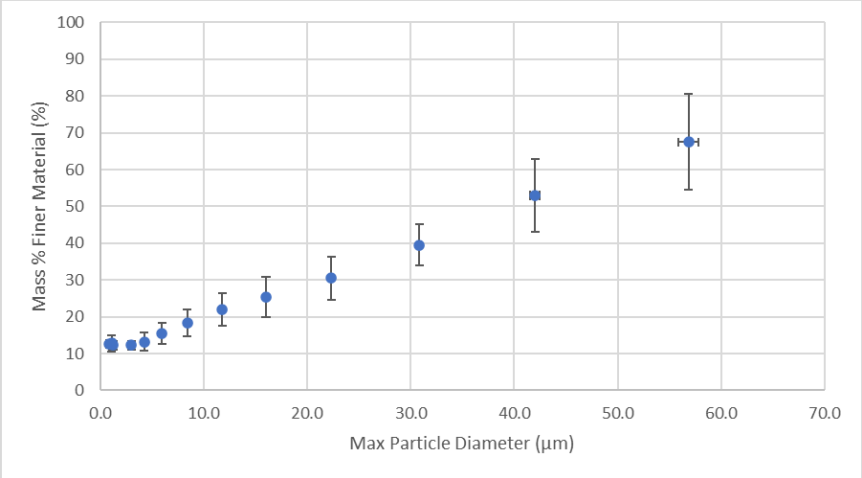


**Figure 2.2.** Particle size distribution of Partrac tracer using hydrometer analysis. Error bars represent a 95% confidence interval.

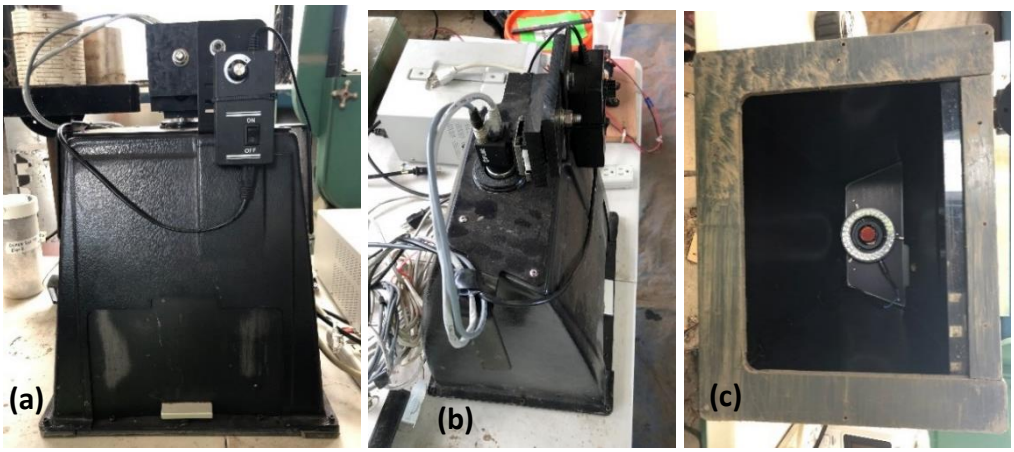


**Figure 2.3.** Collage of photographic hood set up. (**a**) Front with viewing door and black light controls. (**b**) Mounted camera and connection cords. (**c**) Bottom of the hood looking up to view the black light ring and bandpass filter attached to camera.

The soil was obtained from the project's field site at the OSU-Benton County Green Stormwater Infrastructure Research (OGSIR) facility in Corvallis, OR. This soil was found to have a consistent particle size distribution across all the experiments (see Figures 2.4 and 2.5 for the sieving and hydrometer characterization, respectively).

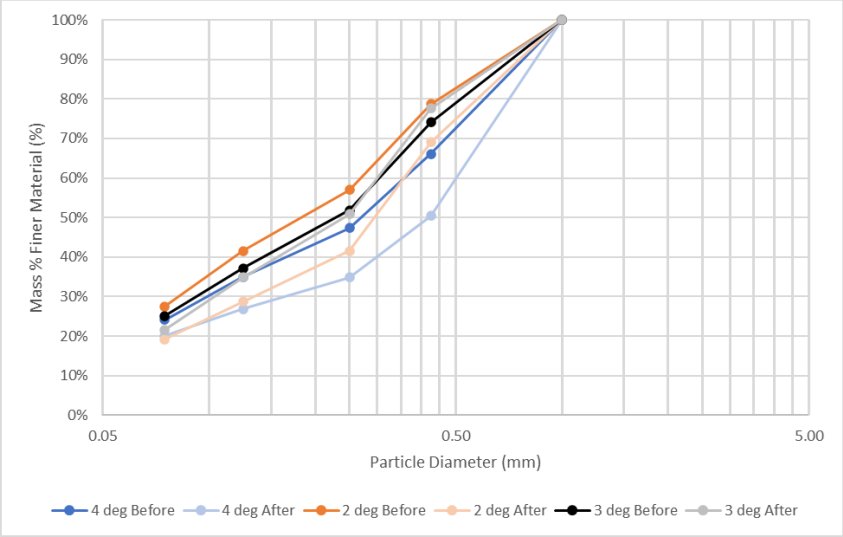


**Figure 2.4.** Particle size distribution from sieving analysis for before and after soil experiment samples, for the fraction of particles >75 µm.

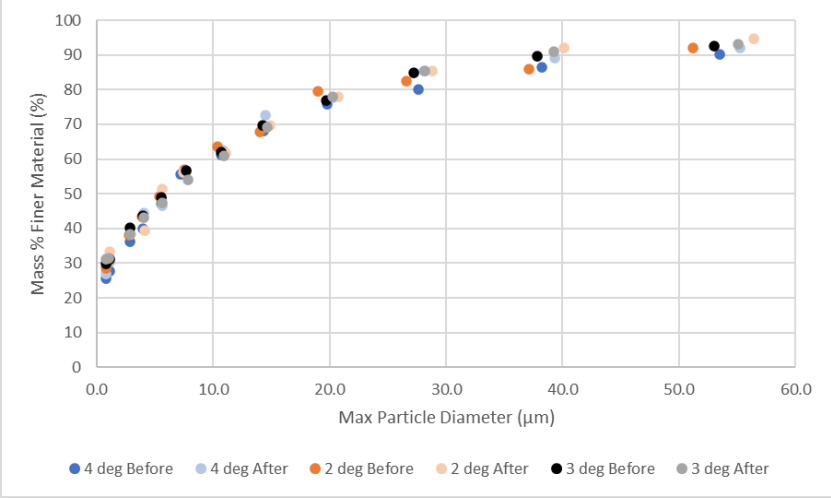


**Figure 2.5.** Particle size distribution from hydrometer analysis for before and after soil experiment samples for the fraction of particles < 75 µm.

To determine the relationship between mass percent of tracer present in a soil sample to fluorescent intensity present in the images, two calibration curves were created (see Figure 2.6). OGSIR soil was added to petri dishes and tracer was then added to reach a desired tracer mass percentage. Samples were manually mixed to create a uniform composition. The petri dish was placed in the camera hood with the black light illuminating the sample, and a photo was captured of the resulting fluorescence. The sample was removed, manually mixed, and imaged two more times, to control for possible variability in mixing. This process was repeated for all calibration points. The images were processed in MATLAB to obtain image intensity values for each photo. The replicate intensities for each calibration point were then averaged and plotted against the known tracer mass percentage. The calibration curves, one for the entire range of 0-100% and a second for the expected field sample range of 0-7% tracer mass, both showed a strong linear trend ($R^2 > 0.98$). This showed the fluorescence in the photos was linearly proportional to the percentage of tracer mass and thus, can act as a proxy for determining the amount of tracer present in field samples.

Due to the non-uniform illumination from the black light, an "intensity calibration" was created to account for brighter and darker areas present in the camera hood sample area. A petri dish filled with tracer was placed in the bottom left corner of the camera hood, imaged, and then shifted half the diameter of the petri dish to the right and imaged again. After reaching the rightmost edge, the dish was moved half the diameter up and subsequently shifted and imaged laterally to the left until reaching the far-left side. The zig-zag process was repeated to create an overlay of all the images that would cover the entire sample area. The results showed a uniform decay of intensity with distance from the center of the image, most likely due to non-uniform illumination by the UV ring-light in the photographic hood apparatus. The corresponding pattern was used to calibrate the experimental flume images by normalizing the intensity such that areas that initially appeared darker would be appropriately brightened during the image intensity analysis discussed in section 2.2.4.

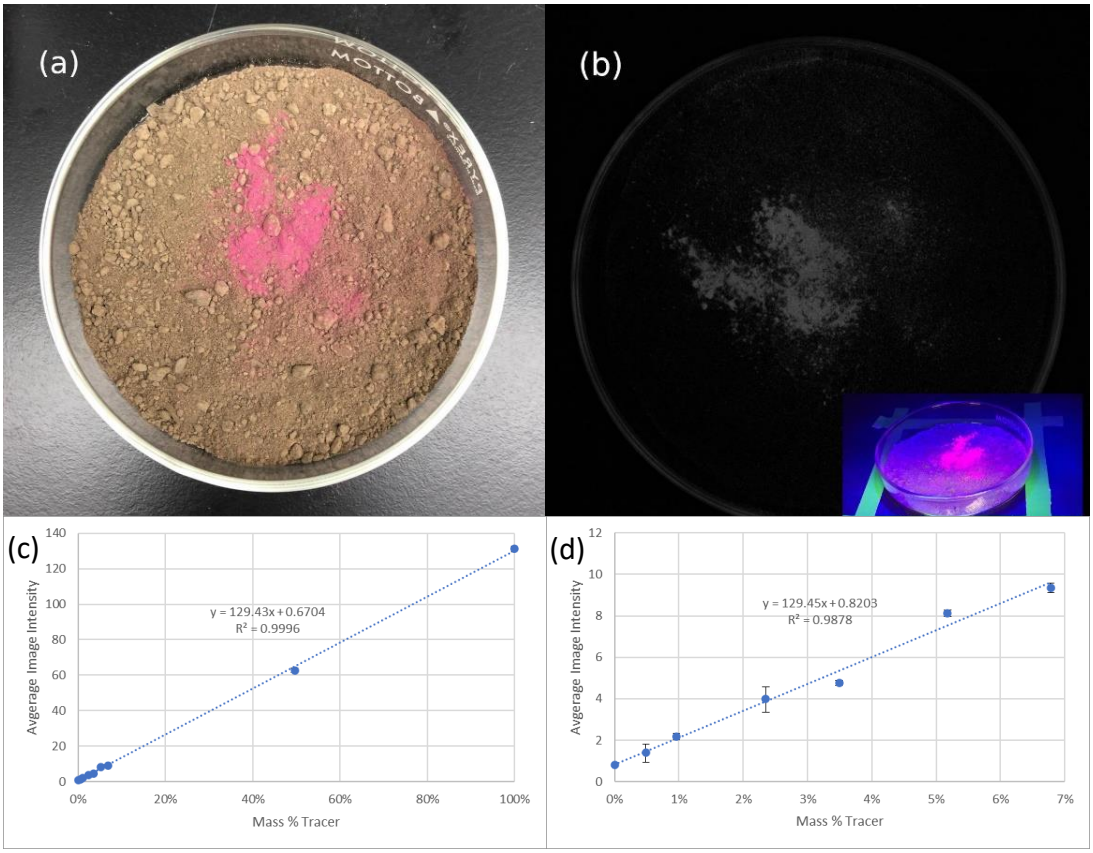


**Figure 2.6.** Calibration of tracer mass percent in soil samples for the image analysis method. (**a**) The tracer particles were added to natural soil in a petri dish, then (**b**) the sample is placed in the camera hood to be imaged under the black light. Note: each sample was well mixed to create a uniform composition; here an un-mixed sample is shown for illustration purposes. (**c**) Calibration curve of the average image intensity vs mass percent of tracer mass for the entire mass percentage range. (**d**) Calibration curve of the average image intensity vs mass percent of tracer mass for the expected mass percentage range in field samples. Note: Error bars for these calibration curves represent a 95% confidence interval.

### 2.2.3 Flume Experiments

Soil collected from OGSIR was dried on a tarp and sifted to remove pebbles. Then it was added in 0.5 cm layers to the flume. After each layer was added , the soil was compacted with a steel tamper. This process was repeated until the soil surface level exceeded the top of the 6" flume end walls. To ensure a uniform and flat surface, a digital level was used to check that variations in bed slope along the width and length of the flume were less than 0.5 degrees. The remaining prepared soil was archived for particle size distribution tests. A scissors jack was installed at the head of the flume for setting the desired bed slope angle. The bed slope was measured in three

locations along the length of the flume with the digital level, and the flume incline was adjusted until the average of these measurements were within ± 0.1 degree of the desired bed slope. The influent tray at the head of the flume was installed to be 0 ± 0.1 degrees to ensure a uniform overflow of tracer-slurry out of the tray. A pre-made tracer paste (2.63 g tracer/1 mL water) was added to the 5-gallon bucket at a concentration of 100 mL of paste for every 4 L of water (final concentration of 65.8 g/L). The flow rate of the pump was measured using a graduated cylinder, and the pump speed was adjusted to achieve an inlet flow of 0.5 ± 0.05 GPM.

Once the flume preparation was complete, tap water was pumped from a separate 5-gallon bucket into the tray. This allowed the flume to be saturated and the top-most layer of soil to be "washed" until a relatively consistent concentration of soil particles was present in the effluent. It was later confirmed using TSS measurements that, after this washing period, the effluent sediment load was constant in time to within 5%. This washing period lasted between 5-9 minutes. To evaluate the background concentration of these soil particles, an effluent water blank sample was collected after a 15 second pulse of flow. This was repeated for a total of four samples. Then the water in the tray was drained and the pump inlet was moved to the tracer slurry bucket. The paint mixer would run for approximately 10 seconds before the pump was activated. The tracer slurry was pumped for 15 seconds after overflowing the tray. Upon completion of each flow pulse, residual water on the flume surface was allowed to drain and the effluent from that pulse was collected. Then the camera hood was placed in the flume where the tracer slurry initially contacts the soil surface and a photo was taken. This was repeated for a total of six images that covered 15 cm intervals (with 50% overlap between successive images) spanning the length of the flume.

The process of flow-pulse and photo data collection was repeated (15 second tracer slurry pulses, with effluent and image collection) five times for a cumulative time of 75 seconds. Once all the time points were completed, the bed slope of the flume and the flow rate of the pump were re-recorded to check for any drift during the experiment. A sample of the tracer slurry was collected as it was overflowing the tray. The water blanks, tracer effluent, and tracer tray samples were stored at room temperature for total suspended solids analysis. The top-most layer of the soil (approximately 1 cm) was scraped off and collected for particle size distribution tests to evaluate any change in soil composition.

The above process was repeated for three bed slopes (2, 3, and 4 degrees), keeping all other parameters constant.

### 2.2.4 Image Intensity Analysis

After completing each experiment, the flume images from each spatial location and time point were compiled in MATLAB. Due to the linear relationship of image intensity and tracer mass (as described in section 2.2.2), the image intensity can be fitted to Equation 2.16 to estimate λ. The analysis for each time point had three parts: 1) compile the photos to produce one seamless image of the entire flume bed, 2) calculate the cross-flume-average image intensity and plot it on a log scale against the distance of the flume, and 3) apply a linear fit to determine the $L_x = 1/\lambda$ parameter and its associated 95% confidence interval. See Figure 2.7 for an output example.

While imaging the surface of the flume with the camera hood was very effective, the base of the frame contacting the surface sediment caused some localized mixing of the deposited tracer into the base sediment. Since the photographic hood was placed in the same locations for each set of measurements, these "smeared" regions occurred at fixed intervals every 15 cm. These areas were excluded from analysis because they would give an inaccurate representation of the deposition profile and skew the calculated $L_x$ parameter.

### 2.2.5 Total Suspended Solids

To estimate the cumulative amount of tracer deposited on the flume, a total suspended solids (TSS) method was used to determine an approximate mass balance. An aluminum tin was weighed on an analytical balance and its mass recorded. Then a 1.0 µm glass fiber filter was placed into the tin and the total mass was recorded. The filter was placed on a vacuum tower with tweezers and set in place with a filter funnel. DI water was added and vacuumed into the collection flask to help seat the filter. The first experimental water blank sample was shaken vigorously to resuspend any sediment present and then quickly poured into a graduated cylinder. After recording the volume in the cylinder, it was added to the filter funnel, and vacuumed through the filter. DI water was used to rinse the sides of the funnel. After all the liquid had

entered the collection flask, the vacuum continued running for an additional one minute, and then turned off. The filter was removed with tweezers and placed back in the respective pre-weighed aluminum tin. The entire process was repeated two more times with the same sample, and then repeated for each sample from the experiment (water blanks, tracer samples, and tracer tray). These were dried in an oven at 105ºC for two hours. After cooling down, each tin plus filter was reweighed and the masses recorded. The TSS was calculated using Equation 2.18:

$$TSS\left(\frac{mg}{L}\right) = \frac{M_A - M_B}{V_f} \tag{2.18}$$

Here $M_A$ is the mass of the tin plus filter after the oven [g], $M_B$ is the mass of the tin plus the filter before the sample was filtered [g], and $V_f$ is the volume of the sample that was filtered [L]. The TSS of the tracer samples were adjusted by subtracting the water blank samples so only the tracer mass was associated with the TSS value.

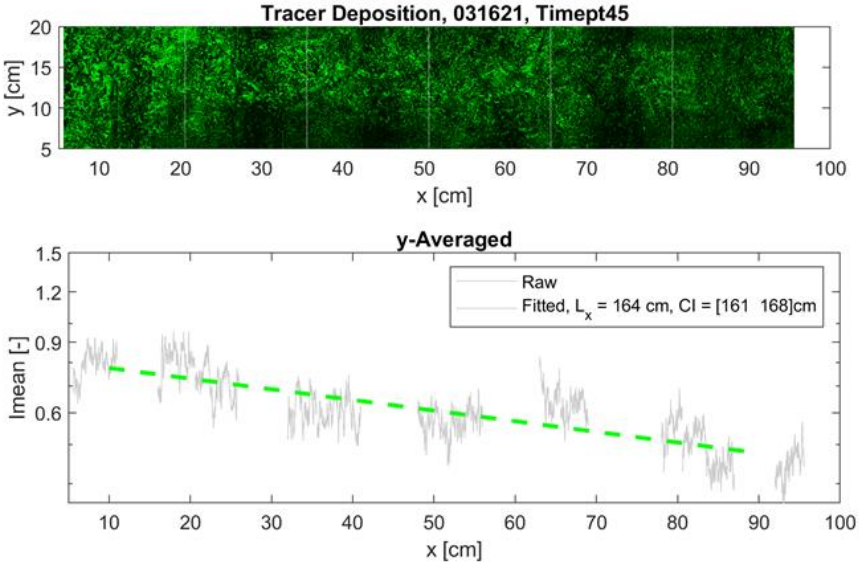


**Figure 2.7.** An example of the MATLAB output for creating a cohesive image of the flume surface and calculating the $L_x$ parameter. This image was produced from the 45 second time point of the 4-degree bed slope experiment. **Top**: Montage of images showing the distribution of tracer deposited on the flume surface (x=0 is the flume inlet). **Bottom**: Across-flume averaged image intensity (gray) fitted to an exponential curve (green). The resulting Lx is shown in the legend, where the CI range in the legend represents a 95% confidence interval.

### 2.2.6 Particle Size Distribution

To determine whether the surface soil properties changed over the course of the experiments, particle size distribution analysis was performed on soil samples collected before and after each experiment. A dry-sieve analysis (for the larger particles) was performed following the ASTM D6913/D6913M method. A mortar and pestle were used to gently break apart any aggregations without grinding larger particles into smaller ones to preserve the existing distribution (following ASTM D7928). Samples were reduced using the quartering method. The sample was then added to a sieve tower containing #18, 40, 60, and 120 sieves. The tower was placed in a ro-tap sieve shaker for 20 minutes. The mass retained on each sieve and within the collection pan was weighed and recorded. The sample in the collection pan was subsequently used in a hydrometer analysis following the ASTM D7928 method.

## 2.3 Results

### 2.3.1 Experimental Calculations for Trapping Efficiency

While samples were collected every 15 seconds for times up to 75 seconds, it was observed that over time the surficial sediment in the flume became saturated with tracer particles. It was apparent this effect altered the surface sediment size distribution and caused a reduction of sediment deposition, i.e. clogging. Inclusion of clogging effects in the analysis would require a time-dependent model for the trapping parameter.[21] However, for the present study we will only focus on the 15-45 second time points so the clogging effects can be neglected. The results from the 60 and 75 second time points will be briefly discussed in section 2.4.3.

Using the $L_x$ values calculated from the image intensity analysis, these were converted to $\lambda$ values for the 15, 30 and 45 second time points of each experiment. Comparisons of the resulting $\lambda$ values are shown in Figure 2.8. These results indicate that with decreasing bed slope there was an increasing removal efficiency, while increasing in cumulative time saw decreasing removal efficiency. Additionally, the relative rates of change in removal efficiency with time were different for each bed slope, where decreasing slope resulted in a faster rate of change. It is also notable that the removal efficiency values appear to converge at the 45 second timepoint.

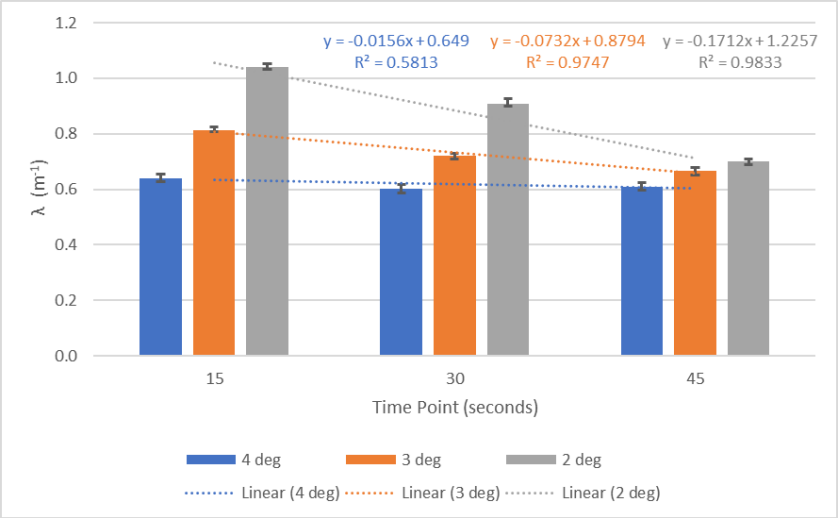


**Figure 2.8.** Removal efficiency values for each slope at different time points. Error bars represent a 95% confidence interval.

### 2.3.2 Deletic Model Calculations for λ

Using the Deletic model (Equations 2.3 to 2.8), the parameters listed in Table 2.1 were calculated for each bed slope. While the change in bed slope impacts the depth of flow (h) and the mean flow velocity (V) calculations, the experimental method kept the flow rate per unit width (q) constant, where q = Vh. Therefore, the Deletic model will only yield one $\lambda_s$ value for all three bed slopes tested. However, the value of $\lambda_s$ from the Deletic model is very similar to the λ values calculated from the intensity image analysis (see Figure 2.9).

**Table 2.1.** Calculated parameter values using Equations 2.3 to 2.8 for determining the removal efficiency per unit length using the Deletic model.

| Parameter | Variable | Units | 4 deg | 3 deg | 2 deg |
|---|---|---|---|---|---|
| Decimal Slope | S | --- | 0.0699 | 0.0524 | 0.0349 |
| Depth of flow | h | mm | 0.89 | 0.97 | 1.09 |
| Stoke's Settling Velocity | $V_s$ | m/s | 0.0014 | | |
| Mean flow velocity | V | m/s | 0.122 | 0.113 | 0.099 |
| Particle fall number | $N_{f,s}$ | --- | 15.65 | 15.47 | 15.71 |
| Trapping efficiency | $T_{r,s}$ | --- | 0.57 | | |
| Trapping efficiency per unit length | $\lambda_s$ | 1/m | 0.47 | | |

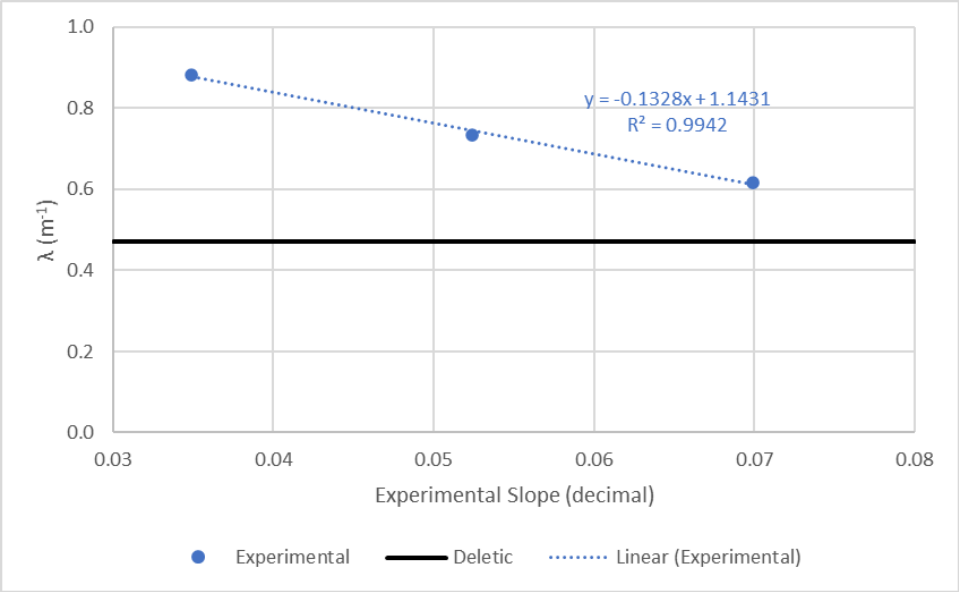


**Figure 2.9.** Comparison of the removal efficiency values from the experimental image analysis vs. the value calculated from the Deletic model.

### 2.3.3 Einstein-Krone Model Calculations for p

Using the parameters calculated in the Deletic model, the probability of the particles depositing on the flume bed (p), can be calculated using the relationship determined from Equations 2.12 and 2.13:

$$p = \frac{\lambda V h}{V_s} \tag{2.19}$$

Here, λ will be the values for each bed slope at every time point calculated from the image intensity analysis and the $\lambda_s$ from the Deletic model. The resulting probability values are shown in Figure 2.10. These results show that with decreasing bed slope there is an increase in probability of particles depositing onto the flume. Once again, the rate of change in probability over time increases with decreasing bed slope and appears to converge at 45 seconds.

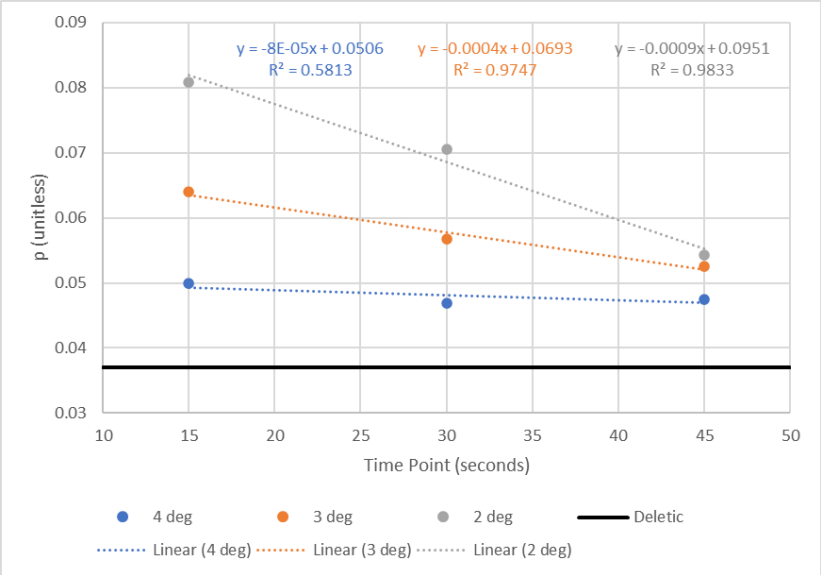


**Figure 2.10.** The probability of particles depositing on the flume bed (p) for each experimental trapping efficiency. The solid black line is the p calculated from Deletic trapping efficiency.

### 2.3.4 Mass Balance

To approximate a mass balance for the tracer deposited onto the flume, two approaches were used: TSS measurements and calculating $D_{tot}$ from Equation 2.17. The TSS measurements were initially in terms of concentration of tracer leaving the flume. To get the deposited concentration in the flume, the effluent concentration was subtracted from the concentration in the tracer tray. This concentration was converted to a mass using the known volumetric flow rate and a flow time of 15 seconds. Figure 2.11 shows the comparison between results from the TSS-determined masses and the masses calculated from $D_{tot}$, for every time point and for each bed slope.

The results from the TSS did not exhibit a trend with respect to bed slope or with time. However, the $D_{tot}$ results indicate an increase of deposited mass with decreasing bed slope, and a convergence at the 45 second time point. Similar to the experimental $\lambda$ results, there is also an increase in the rate of change of mass deposited with decreasing bed slope. While the relative trends are different, the calculated mass deposited using the TSS and $D_{tot}$ calculations are within 0.13 to 0.79 g for each respective time point and bed slope. Since the TSS measurements had an error of approximately 10% (or 0.2 g), this is comparable to the differences seen between the

TSS and $D_{tot}$ values. As discussed further in section 2.4.2, we suggest these discrepancies can be attributed to experimental uncertainty in the TSS mass balance measurements.

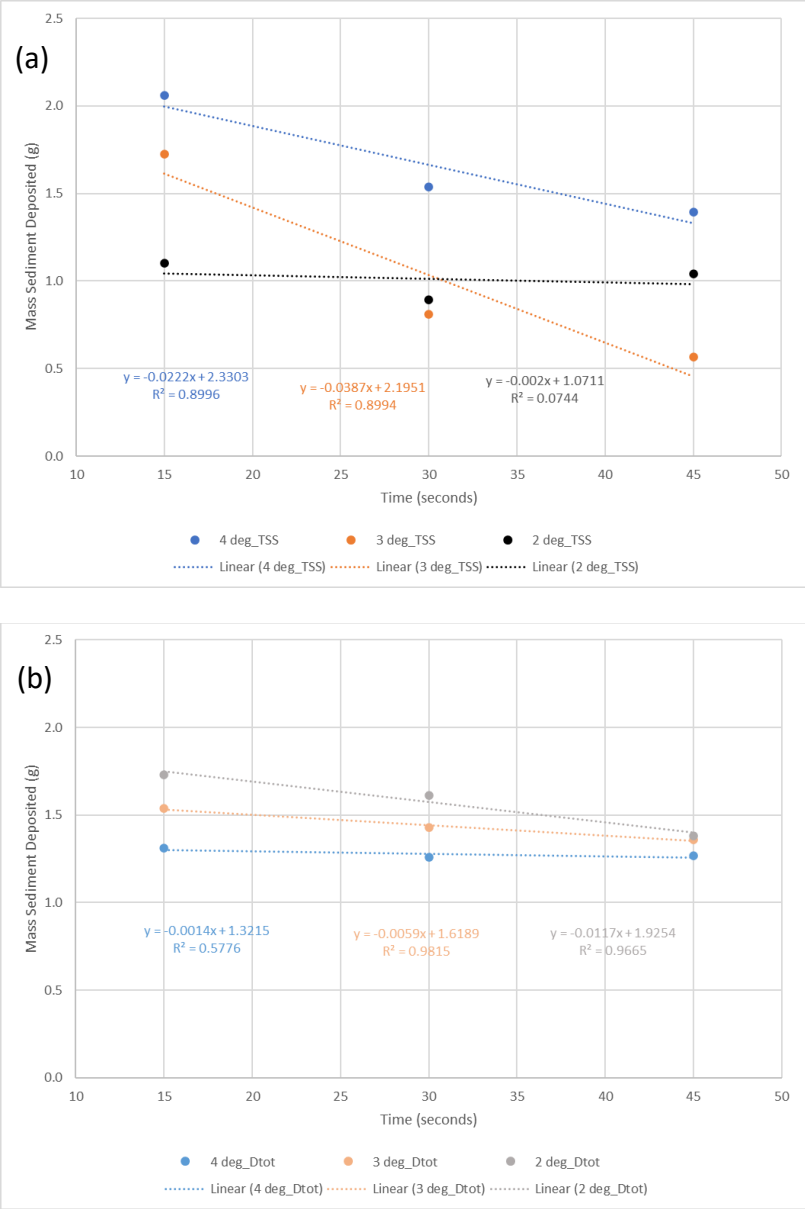


**Figure 2.11**. Determining the mass of sediment deposited at each timepoint to approximate a mass balance using (**a**) TSS measurements and (**b**) D_tot calculations from Equation 2.17.

## 2.4 Discussion

### 2.4.1 Experimental Results vs the Deletic and Einstein-Krone Models

The observed trend of increasing trapping efficiency with decreasing bed slope was not reproduced by the Deletic model but was expected for the present experiments on SEOF flow over a natural soil bed. Since a decrease in bed slope results in a decreased flow velocity, this allows the tracer particles more time to settle through the water and get trapped on the rough soil surface, thus increasing the trapping efficiency. At greater bed slopes, there will also be greater flow velocities that can keep more particles suspended and can re-suspend particles once deposited. Related to this, a decreasing trapping efficiency with time is also to be expected because as more particles deposit over time, the fewer locations are available for the particles to get trapped, i.e. a clogging effect. This would change the dynamics of the deposition process and add another layer of complexity to the models used in this study. It was interesting that the rate of change for the trapping efficiency also increased with decreasing bed slope. This could be due to lower bed slopes having a greater trapping ability so more particles will occupy the "trapping" sites on the soil during a given timeframe when compared to greater bed slopes. Since these sites will be filled up sooner in lower bed slopes, the trapping efficiency should decrease more rapidly due to having fewer locations for the particles to deposit in over time.

When comparing these experimental trapping efficiencies with the Deletic and Einstein-Krone models, there's a few considerations to account for. The Deletic model was designed for applications to grassy bioswales. In this model, l was defined as the length of grass strips the runoff must travel through, whereas this study defined l as the length of the flume. As mentioned in section 2.3.2, the Deletic model is not sensitive to bed slope, but this is most likely due to the use of semi-empirical formulas to derive the trapping efficiency. The lack of bed slope sensitivity evidently is relevant in SEOF flow, possibly because of different physics that dominate sediment deposition. While the alternative probability parameter formulation does not directly include bed slope, it is commonly understood in Einstein-Krone -type models that the probability of deposition (p) is proportional to the bed shear stress, which in turn is directly proportional to bed slope. That is, the increase in bed slope results in a greater shear force that will cause more deposited particles to become resuspended rather than deposited. This yields a decreased probability of particles staying trapped on the surface, thus decreasing the trapping

efficiency. It also would be expected that the deposition probability will decrease with time due to the soil becoming more clogged and leaving fewer possible sites for new particles to deposit.

### 2.4.2 Efficacy of Mass Balance Approaches

While the mass of deposited tracer results for the TSS measurements were similar to the values calculated from $D_{tot}$, the TSS approach did not clearly show a trend with bed slope. This is most likely because the TSS method is sensitive enough to be impacted by small variations within the compacted soil, despite the careful preparation of the flume (see Figure 2.12). The sources of these variations could be from the amount of new soil added, the level of compaction, and degree of saturation. For example, if the soil in one experiment was slightly more compacted, then it would have a lower infiltration rate and stay saturated longer. Thus, the water would flow more quickly down the flume, yielding more water in the effluent and artificially diluting the TSS sample. By contrast, the image analysis method is effectively integrated over the full duration of the deposition phase, hence it is insensitive to transient variations in the flow. The image analysis method also uses curve-fitting to average over small spatial variations that may occur over the length of the flume and offers greater resolution in estimating the deposited mass of tracer. This approach increases the signal-to-noise ratio enough to reveal more mass was deposited at lower bed slopes. This trend agrees with physical expectations since the mass of tracer deposited should be directly related to the trapping efficiency.

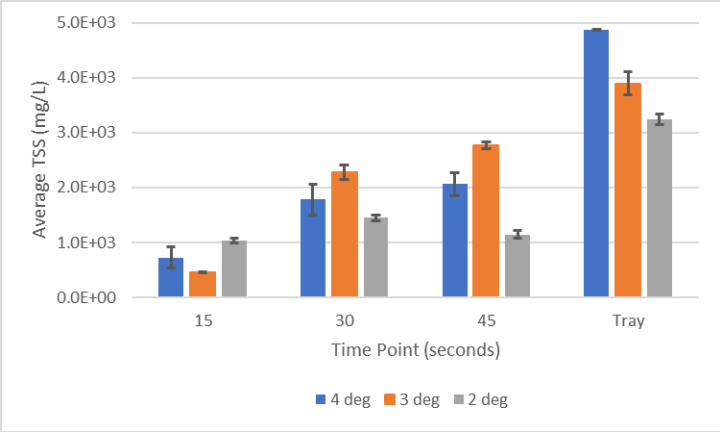


**Figure 2.12.** Average TSS concentration (adjusted with the water blanks) for each bed slope at different time points and slurry tray. Error bars represent a 95% confidence interval.

### 2.4.3 Trapping Efficiencies at Longer Time Points

As mentioned before, these results have primarily focused on the initial three time points of 15, 30, and 45 seconds. However, when the data collected at 60 and 75 seconds is included in the trapping efficiency calculations, the observed trends begin to break down. Figure 2.13 shows the results from the image intensity analysis for all five time points. While there is still a general decreasing trapping efficiency with time, there are few differences at the later time points. At 60 seconds, all three bed slopes approach the same trapping efficiency. This would indicate that the soil surface has started to become clogged, and the trapping efficiency has plateaued. Then at 75 seconds, the trends for each bed slope differ. For four degrees, the trapping efficiency has continued to decrease. At three degrees, it has stayed relatively the same. Then at two degrees it has increased. This increase at two degrees could be due to the erosion or stripping of previously deposited particles that reopen sites for the new tracer particles to deposit in. Or it could be related to the properties of the $L_x$ determination. As $L_x$ increases to be greater than the length of the flume, the slope of the exponential fit decreases, thus decreasing the resolution of observable tracer deposited over a given distance. At this point, the value of $L_x$ becomes unstable due to greater susceptibility to noise in the data. This could explain why the trends suddenly shift between the 60 and 75 time points, where the $L_x$ values range from 150 to 200 cm (approximately 50 to 100% greater than the length of the flume).

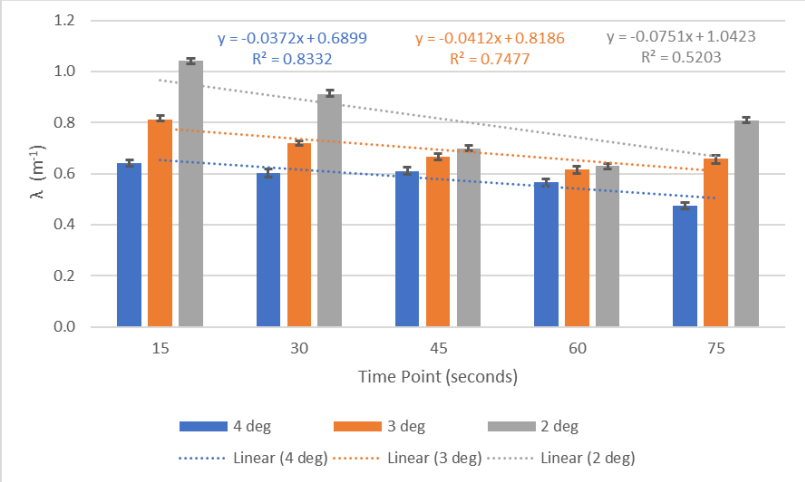


**Figure 2.13.** Removal efficiency values for each bed slope at all measured time points. Error bars represent a 95% confidence interval.

## 2.5 Future Work

One aspect that hasn't been considered in this study, or in the Deletic model, is the effect of infiltration. Due to the high clay content of the soil used for these experiments, the infiltration rate was measured with a single-ring infiltrometer to be less than 0.05 mm/s – far slower than the settling velocity of tracer particles which is on the order of 1 mm/s. Therefore, infiltration was not likely to have a significant influence on sediment deposition in these experiments. However, it would be interesting to repeat the experiments using a soil or sand substrate with higher infiltration rates. It would be expected that higher infiltration will result in greater deposition of particles since saturation would take much longer to achieve, and particles would be encouraged into deposition via the flow into the bed.

Infiltration associated with plants would be another parameter to consider. Due to their roots and stems, plants can increase infiltration by creating preferential flow paths for the water to follow into the subsurface. This scenario was tested using the existing experimental set-up and carefully transplanting an established spreading rush from OGSIR into the middle of the flume. The preliminary results are shown in Figure 2.14. While the plant did not appear to greatly influence the trapping efficiency, it could be that the high clay content (hence low infiltration rate) remained the dominating factor in this case. To determine this in more detail, different plants would need to be tested at each of the bed slopes described here.

A third aspect to investigate would be how the size of the tracer particles change the observed deposition characteristics. As mentioned in the introduction, silt sized (non-clay) particles, like those used in this study, will most likely be impacted by surface filtration and/or straining. However, smaller particles, like clays and colloids, would be more susceptible to physical-chemical mechanisms such as cohesion.[24] Performing additional experiments with different sized tracers, especially with clay particles or colloids, would help determine which depositional processes dominate under a wider range of environmental conditions.

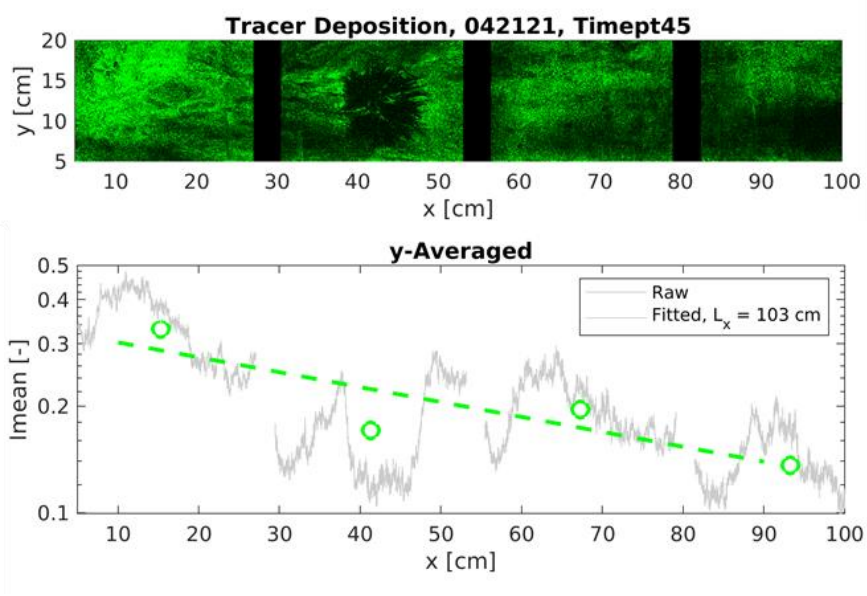


**Figure 2.14.** Image intensity results from a 3-degree bed slope with spreading rush from the 45 second time point. The plant was placed in the flume between 40 and 50 cm.

A final set of parameters that should be experimentally determined are the bed and critical shear forces acting on the flume at each bed slope. Quantifying shear stress would require a measurement of flow rate and flow depth, which is difficult in the SEOF flows considered here. However, these measurements would provide more accurate calculations for the Einstein-Krone probability value and would potentially allow the calculation of the trapping efficiency to include parameters more directly tied to the physical behavior of sediment deposition.

## 2.6 Conclusions

Trapping efficiencies for SEOF were quantified for the first time, using a new method based on fluorescent tracer particles detected photographically. These results were also able to be mathematically modelled using pre-existing models by Deletic and Einstein-Krone. In contrast to the Deletic model, the experimental results showed bed slope does affect the sediment deposition, where lower bed slopes achieve higher trapping efficiencies. Thus, it is important to incorporate parameters directly related to the physics of sediment deposition into mathematical models. One option is to include the Einstein-Krone probability parameter which accounts for

shear forces and the possible resuspension of deposited particles. For calculating a mass balance to determine the mass of tracer deposited, trapping efficiencies and operational parameters can be used. This can also be done using a TSS approach. While the TSS will be more prone to noise and variability, it would provide a good ballpark estimate of deposited mass. To create more realistic models for predicting sediment deposition at field scales, more experiments must be done to account for infiltration rates of soils, shear forces at different bed slopes, and the effect of plants.

## 2.7 Bibliography

(1) Deletic, A. Modelling of Water and Sediment Transport over Grassed Areas. *Journal of Hydrology* **2001**, *248* (1), 168–182. https://doi.org/10.1016/S0022-1694(01)00403-6.

(2) Gu, L.; Dai, B.; Zhu, D. Z.; Hua, Z.; Liu, X.; Duin, B. van; Mahmood, K. Sediment Modelling and Design Optimization for Stormwater Ponds. *Canadian Water Resources Journal / Revue canadienne des ressources hydriques* **2017**, *42* (1), 70–87. https://doi.org/10.1080/07011784.2016.1210542.

(3) LeFevre, G. H.; Paus, K. H.; Natarajan, P.; Gulliver, J. S.; Novak, P. J.; Hozalski, R. M. Review of Dissolved Pollutants in Urban Storm Water and Their Removal and Fate in Bioretention Cells. *J. Environ. Eng.* **2015**, *141* (1), 04014050. https://doi.org/10.1061/(ASCE)EE.1943-7870.0000876.

(4) Li, H.; Davis, A. P. Urban Particle Capture in Bioretention Media. II: Theory and Model Development. *J. Environ. Eng.* **2008**, *134* (6), 419–432. https://doi.org/10.1061/(ASCE)0733-9372(2008)134:6(419).

(5) Ahadi, M.; Bergstrom, D. J.; Mazurek, K. A. Computational Fluid-Dynamics Modeling of the Flow and Sediment Transport in Stormwater Retention Ponds: A Review. *J. Environ. Eng.* **2020**, *146* (9), 03120008. https://doi.org/10.1061/(ASCE)EE.1943-7870.0001784.

(6) Spencer, K. L.; Droppo, I. G.; He, C.; Grapentine, L.; Exall, K. A Novel Tracer Technique for the Assessment of Fine Sediment Dynamics in Urban Water Management Systems. *Water Research* **2011**, *45* (8), 2595–2606. https://doi.org/10.1016/j.watres.2011.02.012.

(7) E. W. Tollner; B. J. Barfield; C. Vachirakornwatana; C. T. Haan. Sediment Deposition Patterns in Simulated Grass Filters. *Transactions of the ASAE* **1977**, *20* (5), 0940–0944. https://doi.org/10.13031/2013.35679.

(8) J. C. Hayes; B. J. Barfield; R. I. Barnhisel. Performance of Grass Filters Under Laboratory and Field Conditions. *Transactions of the ASAE* **1984**, *27* (5), 1321–1331. https://doi.org/10.13031/2013.32966.

(9) Black, K.; Sloan, J.; Gries, T. Everything Goes Somewhere; Tracking the Movement of Contaminated Sediments in an Industrialised Estuary Using Dual Signature Sediment Tracers. *EPJ Web of Conferences* **2013**, *50*, 04001. https://doi.org/10.1051/epjconf/20135004001.

(10) Using Sediment Tracers to Map Sediment Transport Pathways. Partrac, Ltd 2012.

(11) Black, K. S.; Athey, S.; Wilson, P.; Evans, D. The Use of Particle Tracking in Sediment Transport Studies: A Review. *Geological Society, London, Special Publications* **2007**, *274* (1), 73–91. https://doi.org/10.1144/GSL.SP.2007.274.01.09.

(12) Steenhuis, T. S.; Agnew, L.; Gérard-Marchant, P.; Walter, M. T. OVERLAND FLOW. In *Encyclopedia of Soils in the Environment*; Hillel, D., Ed.; Elsevier: Oxford, 2005; pp 130–133. https://doi.org/10.1016/B0-12-348530-4/00568-3.

(13) Stewart, R. D.; Bhaskar, A. S.; Parolari, A. J.; Herrmann, D. L.; Jian, J.; Schifman, L. A.; Shuster, W. D. An Analytical Approach to Ascertain Saturation-Excess versus Infiltration-

Excess Overland Flow in Urban and Reference Landscapes. *Hydrological Processes* **2019**, *33* (26), 3349–3363. https://doi.org/10.1002/hyp.13562.

(14) Pearce, R. A.; Trlica, M. J.; Leininger, W. C.; Smith, J. L.; Frasier, G. W. Efficiency of Grass Buffer Strips and Vegetation Height on Sediment Filtration in Laboratory Rainfall Simulations. *Journal of Environmental Quality* **1997**, *26* (1), 139.

(15) Robinson, C. A.; Ghaffarzadeh, M.; Cruse, R. M. Vegetative Filter Strip Effects on Sediment Concentration in Cropland Runoff. *Journal of Soil and Water Conservation* **1996**, *51* (3), 227–231.

(16) Ligdi, E.; Morgan, R. Contour Grass Strips: A Laboratory Simulation of Their Role in Soil Erosion Control. *Soil Technology* **1995**, *8* (2), 109–117. https://doi.org/10.1016/0933-3630(95)00011-0.

(17) Moskalski, S. M.; Sommerfield, C. K. Suspended Sediment Deposition and Trapping Efficiency in a Delaware Salt Marsh. *Geomorphology* **2012**, *139–140*, 195–204. https://doi.org/10.1016/j.geomorph.2011.10.018.

(18) Bäckström, M. Sediment Transport in Grassed Swales during Simulated Runoff Events. *Water Science and Technology* **2002**, *45* (7), 41–49.

(19) Einstein, H. A. Deposition of Suspended Particles in a Gravel Bed. *Journal of the Hydraulics Division* **1968**, *94* (5), 1197–1206.

(20) Sakthivadivel, R.; Einstein, H. A. Clogging of Porous Column of Spheres by Sediment. *Journal of the Hydraulics Division* **1970**, *96* (2), 461–472. https://doi.org/10.1061/JYCEAJ.0002332.

(21) Cui, Y.; Wooster, J. K.; Baker, P. F.; Dusterhoff, S. R.; Sklar, L. S.; Dietrich, W. E. Theory of Fine Sediment Infiltration into Immobile Gravel Bed. *Journal of Hydraulic Engineering* **2008**, *134* (10), 1421–1429. https://doi.org/10.1061/(ASCE)0733-9429(2008)134:10(1421).

(22) Wooster, J. K.; Dusterhoff, S. R.; Cui, Y.; Sklar, L. S.; Dietrich, W. E.; Malko, M. Sediment Supply and Relative Size Distribution Effects on Fine Sediment Infiltration into Immobile Gravels. *Water Resources Research* **2008**, *44* (3). https://doi.org/10.1029/2006WR005815.

(23) Winston, R. J.; Anderson, A. R.; Hunt, W. F. Modeling Sediment Reduction in Grass Swales and Vegetated Filter Strips Using Particle Settling Theory. *Journal of Environmental Engineering* **2017**, *143* (1), 04016075. https://doi.org/10.1061/(ASCE)EE.1943-7870.0001162.

(24) McDowell-Boyer, L. M.; Hunt, J. R.; Sitar, N. Particle Transport through Porous Media. *Water Resources Research* **1986**, *22* (13), 1901–1921. https://doi.org/10.1029/WR022i013p01901.

(25) Einstein, H. A.; Krone, R. B. Experiments to Determine Modes of Cohesive Sediment Transport in Salt Water. *Journal of Geophysical Research (1896-1977)* **1962**, *67* (4), 1451–1461. https://doi.org/10.1029/JZ067i004p01451.

(26) Arcement, G. J.; Schneider, V. R. *Guide for Selecting Manning's Roughness Coefficients for Natural Channels and Flood Plains*; Water Supply Paper; USGS Numbered Series 2339;

U.S. G.P.O. ; For sale by the Books and Open-File Reports Section, U.S. Geological Survey, 1989; Vol. 2339. https://doi.org/10.3133/wsp2339.

(27) Demonstration of Fluorescent Magnetic Particles for Linking Sources to Sediments at DoD Sites: Partrac Tracer Material ‘White Paper.’ Partrac, Ltd.

# 3. Construction of a Novel Bioswale Design for Improved Contaminant Removal from Stormwater

## 3.1 Introduction

### 3.1.1 Field Site Characteristics

The OSU-Benton County Green Stormwater Infrastructure Research (OGSIR) Facility was built in 2014 to intercept stormwater runoff from a 100,000 $ft^2$ catchment that consists of mostly impermeable asphalt or roof surfaces.[1–3] This catchment receives an average precipitation of 43" per year, which yields an estimated average runoff volume of 2.7 million gallons per year.[3] The main feature of this catchment is the transportation yard of the Benton County Public Works which functions as a storage area for large trucks, road fill material, paint, and a refueling station.[1,2] Many of these materials can act as contaminant sources through fuel leaks and spills, parking lot sediments, and paint spills.[1] See Figure 3.1 for an aerial view of the catchment.

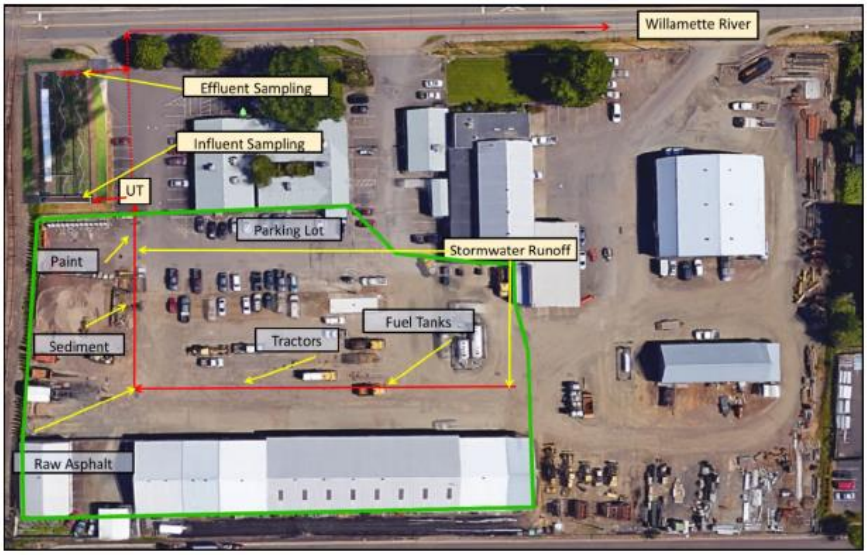


**Figure 3.1** Aerial view of the OGSIR facility and the Benton County Public Works transportation yard. The catchment is outlined in green, the runoff paths are shown in yellow, and the pre-existing city storm drainpipes are shown in red (Source: Kshitiz, 2018).

### 3.1.2 Existing OGSIR Design

The OGSIR facility consists of three bioretention (bioswale) "cells" for testing different treatment technologies for a variety of stormwater contaminants. See Figure 3.2 for a schematic of the facility. The facility begins by intersecting with the existing city stormwater infrastructure pipes. Here, the runoff from the catchment is intercepted and stored in a 1,500-gallon storage tank. A float switch initiates the storage tank sump pump to discharge water from the tank into the 1,500-gallon sediment bay. The residence time of the sediment bay is long enough to allow large particles to settle out the water before overflowing the 45º V-notch weirs, one for each of the three bioretention cells. The cells are 93.3 ft long by 10.5 ft wide by 3 ft deep and utilize an underdrain 4 ft below the top of the cell walls. In case of a severe flooding event, an emergency overflow drain was installed at the end of cells. To prevent infiltration of the runoff directly into the water table, each cell is also self-contained using fish-safe pond liner and geotextile. The cells were filled with different layers of substrate. The layers from top to bottom are 1) an engineered soil mixture of 50% native soil, 25% municipal waste, and 25% mint compost, 2) construction sand, 3) 3/8" gravel, and 4) ¾" crushed river rock. Each cell had a different vegetation configuration. Cell 1 had no vegetation (bare soil), cell 2 contained native grasses, and cell 3 incorporated a mixture of native rushes, sedges, and hedges. Once the water percolates through the vegetation and media layers of the cells, it enters the underdrain and is emptied back into the existing city stormwater piping downstream of the storage tank. This eventually drains into Mill Race stream which discharges into the Willamette River.[1,2,4]

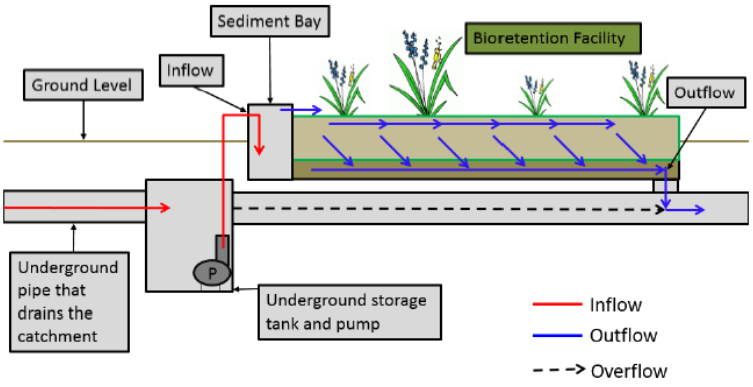


**Figure 3.2** Schematic of a bioretention cell at the OGSIR facility (Source: Livingston, 2015)

### 3.1.3 Water Quality Performance Evaluation of Existing Design

A previous study examined the stormwater treatment performance of the existing bioretention designs three years after opening the facility.[3] The total suspended solids (TSS) and the metals characterization will be the parameters of interest for this chapter. The TSS influent values ranged from 9 – 650 mg/L and had removal rates from 85 – 90%. It was determined that filtration, rather than sedimentation, was the primary mechanism for TSS removal due to the particle size distribution being dominated by fine particles (< 63 μm).

Copper (Cu) and zinc (Zn) were analyzed for total and dissolved metal fractions. The influent concentration of total Cu ranged from 2.4 – 246 ppb and had a removal rate of 54 – 62%. For total Zn, the influent concentration was 60.6 – 286.5 ppb and achieved a removal rate of 61 – 82%. The removal rate for the Cu and Zn particulate fractions were 70 – 83% and 63 – 85%, respectively. For the dissolved fractions, the influent Cu concentrations and resulting removal rates ranged from 1.9 – 14.9 ppb and -59 – 41%, respectively. The influent concentrations and removal rates for Zn ranged from 8.6 – 46.6 ppb and -17 – 86%, respectively. For both dissolved Cu and Zn, the removal performance decreased over time and reached negative removal rates. These trends suggest the dissolved metals previously accumulated in the soil were desorbing and leaching into the stormwater effluent.

While previous studies have shown most metals are associated with particulates and achieve reliable removal rates, there are still concerns with removal of dissolved metal due to the limited capabilities of bioretention systems to strongly sorb these contaminants.[5,6] Other studies have found that dissolved metals do have the potential to leach out bioretention systems, especially when the influent stormwater concentrations exceed the soil's sorption capacity.[6–8] These literature findings corroborate the observed leaching of Cu and Zn from the OGSIR facility.

### 3.1.4 Sorbent Amendments for Stormwater Applications

To address these metal leaching contaminant concerns, recent studies have investigated the use of various sorbents as amendments for treating stormwater.[9–12] Biochar has become a popular sorbent in contaminant removal studies.[13–16] Biochar is a carbonaceous material produced by thermochemical (e.g. pyrolysis, gasification) conversion of agricultural, feedstock, or sludge

biomass.[13] Some characteristics that make biochar an attractive option for contaminant treatment in environmental applications include large adsorption capacity, high specific surface area, and ion exchange capacity.[13] Biochar has been shown to effectively remove inorganic (e.g. heavy metals, nitrate, sulfide) and organic contaminants (e.g. nutrients, pesticides, antibiotics), including emerging contaminants of concern like polycyclic aromatic hydrocarbons (PAHs) and polychlorinated biphenyls (PCBs).[13,15,16]

While commercially available sorbents can treat a variety of the common stormwater contaminants, polyfluoroalkyl substances (PFAS), an emerging set of contaminants, have been difficult to remove from the environment.[17,18] However, a new sorbent, RemBind®, was recently developed specifically for the remediation of PFAS.[19] RemBind® is a blend of aluminum hydroxide, carbon, and clay that can be used in a powder or particulate form.[19] The powdered form is for soil remediation or wastewater treatment applications.[19] As a particulate, it can be installed as a passive reactive barrier for treating groundwater contamination.[19]

### 3.1.5 New Treatment Train Design

After analyzing the performance data of the existing bioretention design, faculty from the College of Engineering collaborated to design and implement a new gravity-fed bioswale system. Instead of solely relying on bioretention, this new system incorporates a treatment train approach, with a traditional bioswale followed by two sets of sorbents: biochar and RemBind®. Going forward, this design will be called the "treatment train." The treatment train was installed in cell 1, the bare-soil bioswale, to utilize the existing infrastructure. See Figure 3.3 for schematics of the treatment train design.

The stormwater influent will still be collected from the transportation yard catchment and diverted into the underground storage basin. Then the water bypasses the sedimentation basin and is directly routed into the first riser (junction 0) via a hose. The water entering this riser is controlled by a globe valve that is manually adjusted for a desired flow rate. Once the riser is filled, the water spills over a Thelmar Wier, which is used to as a secondary method for measuring the flow rate entering the LID. From there, the water will travel into a perforated hose and drain out across the top surface of the bioretention "LID" cell. The water will infiltrate

through the soil media and leave the LID via a perforated underdrain into the second riser (junction 1).

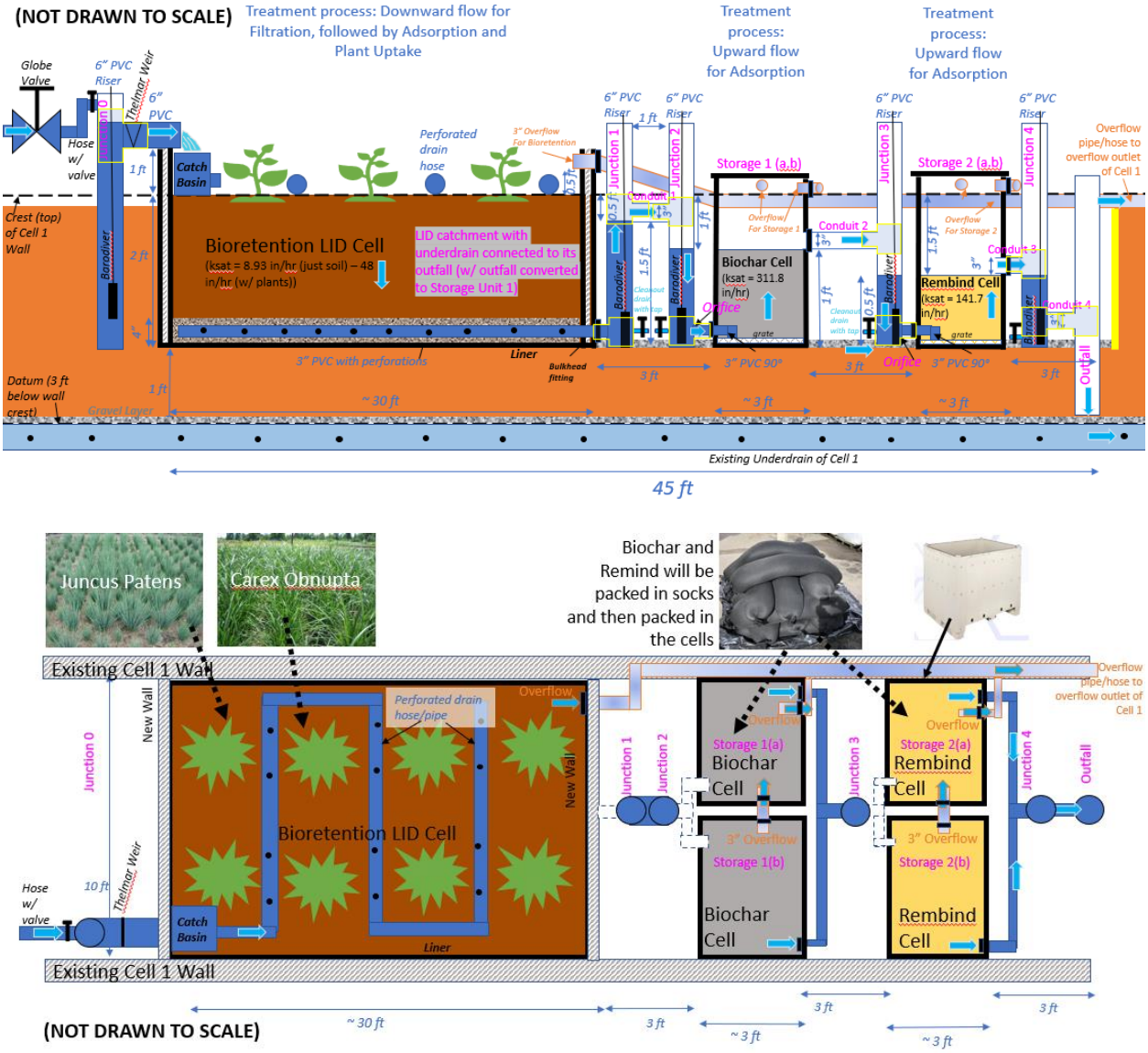


**Figure 3.3** Schematic views of the new treatment train design. **Top:** Profile view of system to showcase the direction of water flow and the installation into the pre-existing structure in Cell 1. **Bottom:** Aerial view of the system to illustrate the orientation of the perforated hose for water distribution throughout the LID and the use of two macro-bins for each sorbent. Created by Dr. Meghna Babbar-Sebens, 2020.

After filling the second riser, the water will enter a third riser (junction 2). The purpose of this riser is to invert the water flow to achieve an up-flow through the sorbent "macro-bins." The third riser also splits the flow between the two biochar macro-bins. Once both biochar bins are saturated, the water from the bins will enter the fourth riser (junction 3) to be re-mixed before the flow is divided into the two RemBind® bins. Then, effluent from these bins will be rejoined at the fifth riser (junction 4) before exiting the treatment train through an outfall pipe that connects to the existing underdrain of the bioretention cell. This transports the water out to the city's stormwater piping, just like the effluent from cells 2 and 3.

There are several short-term and long-term objectives for this project. In the short-term, we will 1) construct the treatment train and 2) establish a water sampling regime. For the long-term, the team will 1) collect water samples during storm events to track contaminant removal after each stage of the treatment train, 2) compare the treatment train removal efficiencies with those from the bioswale systems in cells 2 and 3, and 3) evaluate how the treatment performance changes as the system ages. The short-term objectives will be discussed in the section 3.2 while the plan for fulfilling the long-term objectives will be described in section 3.3.

## 3.2 Methods and Materials

### 3.2.1 Treatment Train Construction

Excavation of cell 1 was completed in late November 2020, where approximately two feet of soil was removed and stored on-site. Then the macro-bins were installed by digging shallow trenches to bury the feet. The macro-bins are 39" long by 46.75" wide by 42.5" tall and are made of inject-molded, high impact resistant plastic. These bins were chosen because they are commonly used in food applications, which reduced the risk of constituents leaching out of the bin and contaminating the stormwater. Next, the LID was constructed using a wood frame reinforced with metal plating and secured to the walls of cell 1. Then, the LID was waterproofed by installing and sealing large sections of geotextile and pond liner to the frame. The underdrain was created using perforated 3" PVC piping and laid in a T-shape, with the top of the T placed at the far end of the LID. The PVC was also wrapped in geotextile to prevent clogging of the underdrain from fine soil particulates.

In January 2021, the LID was filled with the layers of soil media. First, a 3" layer of smooth river rock was added. Then a 2" layer of sand was added and compacted. Note, a layer of geotextile was placed in between the river rock and the sand to ensure the sand would not shift and lodge in the pore spaces of the rock. Over the next week, the LID was filled with the soil removed during the excavation. The perforated hose was placed on top of the soil in a winding configuration to uniformly distribute the incoming stormwater. Finally, approximately 15 spreading rushes and 15 slough sedges were planted in the LID. Both plants are native to the Willamette Valley and have been successful over the past six years in cell 2. See Figure 3.4 for a series of progress photos from the LID construction.


**Figure 3.4** Progress photos taken during construction of the LID. (**a**) Cell 1 before excavation. (**b**) Completed LID frame. (**c**) Installation of pond liner and underdrain. (**d**) River rock layer. (**e**) Compacted sand layer. (**f**) OGSIR soil with perforated hose, native vegetation, and mulch.

The vertical risers were made from 6” PVC pipes that are installed approximately 4” into the ground. Lateral wooden cross-pieces were later added to provide extra support so the additional weight of the water in the risers would not cause them to lean or tilt. Each riser is equipped with two sensors, 1) a baro-diver for creating the hydrograph at each section of the treatment train and 2) turbidity sensors for monitoring suspended particulate concentrations. Holes were drilled into the macro bins for the PVC connections to the risers. These holes and PVC connections were carefully configurated to allow the system to be gravity fed.

Construction of the treatment train was completed in early February 2021 after each sorbent, biochar and RemBind®, was separately packed into fabric “socks.” These socks will be placed in alternating 90-degree layers (like Lincoln Logs) in their corresponding macro bins. The biochar socks were officially installed in the first macro bins in April 2021. Prior to exposure to a storm event, the socks were rinsed with city water to flush out any leaching particles or dissolved constituents. Once the biochar socks have been adequately washed, the RemBind® socks will be added to the downstream bins. See Figure 3.5 for a series of images showcasing the treatment train after construction was completed.


**Figure 3.5** Photos of competed treatment train. Note: water flows start at the riser in image c and end at the far left riser in image a. (**a**) Sorbent boxes with risers 4 and 5. Biochar socks are in the right bins and RemBind® are in the left bins. (**b**) Outlet of LID with risers 2 and 3 connecting to the biochar sorbent boxes. (**c**) Vegetated LID with perforated hose and inlet riser 1.

### 3.2.2 Stormwater Sampling Plan

Stormwater samples will be collected at risers 1, 2, 4, and 5. Water from riser 1 will provide the influent characterization. Risers 2, 4, and 5 will be used to track changes in the stormwater

constituent concentrations after the LID, biochar, and RemBind®, respectively. ISCO 6712 automated samplers will be used to collect water samples during storm events. One ISCO will be deployed at each riser, with the end of the inlet tubing placed at the same elevation of the bottom of the outlet pipe connection. Before collecting samples, each ISCO must be calibrated for the desired collection volume. Then a field blank sample will be collected by pumping deionized water through the ISCO. This sample will determine the background levels of any constituents that are present due to the equipment and not the stormwater. Acid-washed ISCO bottles are placed in the bottom of the autosampler and ice is added around the bottles to preserve the water samples until they can be taken to the lab. The ISCO will be programed on a time interval basis, with 500 mL samples collected every 30 minutes. Each bottle will only contain one water sample. This allows the ISCO to sample a storm event for up to 24 hours. During a storm, volunteers will also collect live *in situ* measurements of temperature, pH, and total dissolved solids (TDS) at each riser. These live measurements can be used to corroborate the laboratory analysis of the samples collected by the ISCO. After a storm event has ended, the bottles will be numbered according to their placement in the ISCO, capped, transported in a cooler with more ice to the lab, and stored at 4ºC.

## 3.3 Future Work

Due to the timing of treatment train construction, only one small spring storm was able to be sampled. This storm acted as a practice run for deploying the ISCO and processing collected stormwater samples. During fall term 2021, there are plans to sample a least three storms. Flow-weighted composites will be created manually for each sampling location using the hydrographs. These composite samples will be analyzed for TSS, TDS, hardness, alkalinity, nutrients, nitrate, nitrite, carbonaceous oxygen demand (COD), and total and dissolved metals (copper and zinc). The TSS and TDS measurements will utilize a vacuum filtering system with glass microfiber filters with a nominal 0.7 µm pore size. The hardness, alkalinity, nutrients, nitrate, nitrite, and COD measurements will be performed using Hach kits. Metals analysis will be performed with an inductively coupled plasma mass spectrometer (ICP-MS).

The laboratory results for each sampling location for a given storm event will be evaluated to determine the treatment performance at each stage of the treatment train. This storm-specific approach will show which contaminants are removed and to what extent when flowing through the bioretention, biochar, and RemBind®. The fall storm results will also be compared to the findings presented by Kshitiz, 2018. Comparing the overall performance of the treatment train with the traditional bioretention designs will offer an opportunity to gauge the effectiveness of adding biochar and RemBind® under field conditions. A final years-long objective is evaluating changes in treatment performance as the system "ages." Since most bioretention systems do not have their effluent water quality monitored, it would be interesting to observe how removal efficiencies for a variety of contaminants shift over time.

## 3.4 Conclusions

Stormwater quality concerns regarding the leaching of dissolved contaminants, such as heavy metals, can be addressed by incorporating commercial sorbents into bioretention systems. A new bioswale design utilizing a treatment train approach with biochar and RemBind® was successfully installed at the OGSIR facility. Deploying automated water samples at each stage of the treatment train will provide valuable insight into where and to what extent stormwater contaminants will be treated in this system. Comparing these results to historical data from the adjacent cells at OGSIR will provide context for whether the treatment train is achieving better treatment performances compared to traditional bioretention designs. A valuable long-term study would be monitoring how treatment performance changes as the treatment train and conventional bioswales age over a multi-year time scale. Observing changes in treatment performance over time could better inform maintenance requirements and forecasted lifetimes of bioretention systems. This would enable communities to continue protecting their natural water quality for generations to come.

## 3.5 Bibliography

(1) OGSIR Facility Design http://research.engr.oregonstate.edu/hydroinformatics/avery/facilitydesign.

(2) Livingston, G. Bioretention Establishment Hydrologic Characterization with Drift Correction and Calibration of Fine Water Level Measurements, Oregon State University, Corvallis, OR, USA, 2015.

(3) Gyawali, K. Characterization of Stormwater Runoff from a County Maintenance Facility and Evaluation of Temporal Performance of Bioswale in Its Treatment, Oregon State University, Corvallis, OR, USA, 2018.

(4) Livingston, G. *Stormwater Solutions - a Documentary Film on the OGSIR Facility*; Corvallis, OR, USA.

(5) LeFevre, G. H.; Paus, K. H.; Natarajan, P.; Gulliver, J. S.; Novak, P. J.; Hozalski, R. M. Review of Dissolved Pollutants in Urban Storm Water and Their Removal and Fate in Bioretention Cells. *J. Environ. Eng.* **2015**, *141* (1), 04014050. https://doi.org/10.1061/(ASCE)EE.1943-7870.0000876.

(6) Roy-Poirier, A.; Champagne, P.; Filion, Y. Review of Bioretention System Research and Design: Past, Present, and Future. *Journal of Environmental Engineering* **2010**, *136* (9), 878–889. https://doi.org/10.1061/(ASCE)EE.1943-7870.0000227.

(7) Davis, A. P.; Shokouhian, M.; Sharma, H.; Minami, C. Water Quality Improvement through Bioretention Media: Nitrogen and Phosphorus Removal. *Water Environ Res* **2006**, *78* (3), 284–293. https://doi.org/10.2175/106143005x94376.

(8) Sun, X.; Davis, A. P. Heavy Metal Fates in Laboratory Bioretention Systems. *Chemosphere* **2007**, *66* (9), 1601–1609. https://doi.org/10.1016/j.chemosphere.2006.08.013.

(9) Huber, M.; Badenberg, S. C.; Wulff, M.; Drewes, J. E.; Helmreich, B. Evaluation of Factors Influencing Lab-Scale Studies to Determine Heavy Metal Removal by Six Sorbents for Stormwater Treatment. *Water* **2016**, *8* (2), 62. https://doi.org/10.3390/w8020062.

(10) Genç-Fuhrman, H.; Mikkelsen, P. S.; Ledin, A. Simultaneous Removal of As, Cd, Cr, Cu, Ni and Zn from Stormwater: Experimental Comparison of 11 Different Sorbents. *Water Research* **2007**, *41* (3), 591–602. https://doi.org/10.1016/j.watres.2006.10.024.

(11) Wu, P.; Zhou, Y. Simultaneous Removal of Coexistent Heavy Metals from Simulated Urban Stormwater Using Four Sorbents: A Porous Iron Sorbent and Its Mixtures with Zeolite and Crystal Gravel. *Journal of Hazardous Materials* **2009**, *168* (2), 674–680. https://doi.org/10.1016/j.jhazmat.2009.02.093.

(12) Björklund, K.; Li, L. Sorption of Organic Pollutants Frequently Detected in Stormwater: Evaluation of Five Potential Sorbents. *Environ Technol* **2018**, *39* (18), 2335–2345. https://doi.org/10.1080/09593330.2017.1354924.

(13) Oliveira, F. R.; Patel, A. K.; Jaisi, D. P.; Adhikari, S.; Lu, H.; Khanal, S. K. Environmental Application of Biochar: Current Status and Perspectives. *Bioresource Technology* **2017**, *246*, 110–122. https://doi.org/10.1016/j.biortech.2017.08.122.

(14) Alam, M. Z.; Anwar, A. H. M. F. Nutrients Adsorption onto Biochar and Alum Sludge for Treating Stormwater. *J. of Wat. & Envir. Tech.* **2020**, *18* (2), 132–146. https://doi.org/10.2965/jwet.19-077.

(15) Min, S.; Huang, M.; Zhang, W.; Wu, C.; Sun, H. A Pilot Bioretention System with Commercial Activated Carbon and River Sediment-Derived Biochar for Enhanced Nutrient Removal from Stormwater. *Water Science and Technology* **2019**, *80* (4), 707–716. http://dx.doi.org.ezproxy.proxy.library.oregonstate.edu/10.2166/wst.2019.310.

(16) Palansooriya, K. N.; Yang, Y.; Tsang, Y. F.; Sarkar, B.; Hou, D.; Cao, X.; Meers, E.; Rinklebe, J.; Kim, K.-H.; Ok, Y. S. Occurrence of Contaminants in Drinking Water Sources and the Potential of Biochar for Water Quality Improvement: A Review. *Critical Reviews in Environmental Science and Technology* **2020**, *50* (6), 549–611. https://doi.org/10.1080/10643389.2019.1629803.

(17) Pramanik, B. K.; Roychand, R.; Monira, S.; Bhuiyan, M.; Jegatheesan, V. Fate of Road-Dust Associated Microplastics and per- and Polyfluorinated Substances in Stormwater. *Process Safety and Environmental Protection* **2020**, *144*, 236–241. https://doi.org/10.1016/j.psep.2020.07.020.

(18) Hu, X. C.; Andrews, D. Q.; Lindstrom, A. B.; Bruton, T. A.; Schaider, L. A.; Grandjean, P.; Lohmann, R.; Carignan, C. C.; Blum, A.; Balan, S. A.; Higgins, C. P.; Sunderland, E. M. Detection of Poly- and Perfluoroalkyl Substances (PFASs) in U.S. Drinking Water Linked to Industrial Sites, Military Fire Training Areas, and Wastewater Treatment Plants. *Environ. Sci. Technol. Lett.* **2016**, *3* (10), 344–350. https://doi.org/10.1021/acs.estlett.6b00260.

(19) RemBind is a Binding Agent for PFAS Remediation in Soil and Water https://rembind.com/uploads/Z070-15-RemBind-Product-Overview.pdf.

# 4. Conclusion

As researchers learn more about stormwater contaminant removal techniques at a laboratory level, it is important to translate these findings into innovating stormwater management technologies at field scales. In chapter two, trapping efficiencies for stormwater runoff under shallow excess overland flows were quantified for the first time, using a new fluorescent image intensity analysis approach in a small flume. Since the bed slope angles used in the sediment tracer study are consistent with the bed slopes at OGSIR, the lab-scale sediment deposition behaviors can be applied to the full-scale bioswales and the new treatment train at OGSIR. These findings will allow the OGSIR team to predict where silt-sized particles will accumulate in the system so preventative maintenance can be conducted to mitigate clogging of the soil surface and decreasing the infiltration rate, which is critical to the treatment of other contaminants.

Field-scale studies are an invaluable component of stormwater research because they can provide information on complex environmental conditions and parameters that cannot be effectively replicated in a laboratory or incorporated into a model. This situation greatly impacted the comparison of the experimental tracer results to pre-existing models. Lacking the inclusion of physical properties of sediment deposition, like bed shear stress, one of these models failed to predict that bed slope would affect the trapping efficiency of sediment particles. Incorporating more field-generated data, like sediment deposition and dissolved contaminant removal, can drastically improve the applicability and accuracy of predictive models related to bioretention systems. In turn, these models can be used to design environmentally responsible stormwater management systems that improve community health by protecting natural water sources from particulate and dissolved contaminants found in stormwater runoff.